Geochimical segmentation of the Mid-Atlantic Ridge north of Iceland and ridge-hot spot interaction in the North Atlantic

Janne Blichert-Toft, Arnaud Agranier, Magdalena Andres, Richard Kingsley, Jean-Guy Schilling, Francis Albarède

Geochemistry Geophysics Geosystems G3
AN ELECTRONIC JOURNAL OF THE EARTH SCIENCES
Published by AGU and the Geochemical Society

Article
Volume 6, Number 1
14 January 2005
Q01E19, doi:10.1029/2004GC000788
ISSN: 1525-2027

Geochemical segmentation of the Mid-Atlantic Ridge north of Iceland and ridge–hot spot interaction in the North Atlantic

Janne Blichert-Toft and Arnaud Agranier
Ecole Normale Supérieure, 46 Allée d'Italie, 69364 Lyon Cedex 7, France (jblicher@ens-lyon.fr)

Magdalena Andres, Richard Kingsley, and Jean-Guy Schilling
Graduate School of Oceanography, University of Rhode Island, South Ferry Road, Narragansett, Rhode Island 02882, USA

Francis Albarède
Ecole Normale Supérieure, 46 Allée d'Italie, 69364 Lyon Cedex 7, France

[1] Hafnium, Nd, and Pb isotope data are reported for mid-ocean ridge basalts (MORB) from the Mid-Atlantic Ridge between 50°N and 78°N. Treating Pb isotopes separately from Sr, Nd, and Hf isotopes drastically reduces the number of end-members required to account for mixing properties in the investigated basalt population. Three geochemical end-members account for >99.95% of the observed Pb isotope variability. The isotopic compositions of Pb are somewhat decoupled from those of other isotopic systems due to nonlinear mixing relationships between isotopic compositions of different elements and elemental fractionation by magmatic processes. The first principal component reflects a mixture of two geochemical end-members, DM and the common component C. The third end-member (EM) is enriched and its Th/U ratio substantially higher than that of the first two end-members. The HIMU end-member apparently is missing. Iceland and Jan Mayen divide the northern Mid-Atlantic Ridge into three isotopically distinct segments. The strong first Pb principal component present in Icelandic basalts expands southward into the Reykjanes Ridge, but not northward into the Kolbeinsey Ridge. Similar features are observed for Hf and Nd isotope compositions. By contrast, the second Pb principal component shows a smooth transition between Kolbeinsey MORB and subaerial Iceland data. The distribution of the two Pb principal components present in the basalts around Jan Mayen likewise is contrasted: the first Pb principal component and its Nd and Hf counterparts flow northward into the Mohns Ridge but are arrested southward by the Jan Mayen fracture zone. Basalts north of Jan Mayen display the most radiogenic Hf reported so far for any MORB worldwide. For ~1000 km along the Mohns and Knipovich Ridges, Hf isotope compositions fail to correlate linearly with ε_{Nd}, but instead define a hyperbolic array between the C component and an end-member unusually depleted in Hf. The latter carries a strong garnet signature and may appear by disequilibrium melting of streaks of subcontinental lithosphere left by continental rifting. The presence of continental crust beneath Jan Mayen is not supported by either Ce/Pb, Nb/U, or Hf/Sm. If Jan Mayen is a hot spot, its material is injected along a major mantle discontinuity separating distinct convective domains.

Components: 18,022 words, 14 figures, 2 tables.

Keywords: Mid-Atlantic Ridge; MORB; Hf isotopes; Pb isotopes; hot spot; garnet fractionation; mantle boundary.

Index Terms: 1025 Geochemistry: Composition of the mantle; 1040 Geochemistry: Radiogenic isotope geochemistry.

Received 30 June 2004; **Revised** 1 November 2004; **Accepted** 10 November 2004; **Published** 14 January 2005.

Blichert-Toft, J., A. Agranier, M. Andres, R. Kingsley, J.-G. Schilling, and F. Albarède (2005), Geochemical segmentation of the Mid-Atlantic Ridge north of Iceland and ridge–hot spot interaction in the North Atlantic, *Geochem. Geophys. Geosyst.*, *6*, Q01E19, doi:10.1029/2004GC000788.

Theme: Plume-Ridge Interaction **Guest Editor:** David Graham

1. Introduction

[2] A conspicuous indication that some parts of the mantle are geochemically distinct laterally was demonstrated by *Dupré and Allègre*'s [1983] observation that volcanic ocean islands from the South Atlantic and Indian Oceans have anomalous Pb isotope compositions and form a coherent geochemical province, which *Hart* [1984] dubbed the Dupal anomaly. Assuming that volcanism from ocean islands is controlled by melting of deep mantle material, such a broad-scale geochemical provinciality may be interpreted as the surface expression of lower mantle heterogeneities, a concept that *Castillo* [1988] related to domains of low seismic velocities. Major geochemical discontinuities were later identified along the Antarctic Ridge, where the Australian-Antarctic Discontinuity seems to separate two distinct domains of the upper mantle that convect separately [*Klein et al.*, 1988; *Kempton et al.*, 2002; *Hanan et al.*, 2004], and the East Pacific Rise, where the Easter Microplate appears to divide two discrete types of Pacific upper mantle [*Vlastélic et al.*, 1999]. Documenting the existence of such heterogeneities is important because they provide prime evidence that long-term geochemical structures may survive mantle convection and thereby lend themselves as a means for placing constraints on the efficiency of convective stirring. This in turn is critical because time and length scales inherent to most current models of tracer dispersion in mantle convection [e.g., *Gurnis and Davies*, 1986; *Christensen and Hofmann*, 1994; *Ferrachat and Ricard*, 1998; *van Keken and Ballentine*, 1998; *Davies*, 2002; *Tackley and Xie*, 2002] are still poorly constrained and thus remain in need of proper scaling by measurement and observation.

[3] Because the local upper mantle beneath the Arctic Mid-Atlantic Ridge (MAR) is still under the influence of recent continental breakup and also is affected by the Iceland hot spot activity, it is a favorable location for studying the different scales of geochemical mantle heterogeneity. Among factors that contribute to these heterogeneities in the North Atlantic upper mantle, the following are of particular importance:

[4] 1. The North Atlantic oceanic passage opened up only ~54 Myr ago.

[5] 2. Continental breakup coincided with the emplacement of the vast Brito-Arctic province of flood basalts, which covers the north of the British Isles, East Greenland and the submarine flows of the Seaward-Dipping Reflector Sequences of the Vøring Bank [*Eldholm et al.*, 1989], and the East Greenland margin [*Larsen and Saunders*, 1998].

[6] 3. Relatively slow spreading rates keep the oceanic gap between Greenland and Europe rather narrow.

[7] 4. The absolute displacement of the lithosphere, in particular that of Europe, over the fixed hot spot frame is fairly slow [*Gripp and Gordon*, 2002].

[8] The general bathymetry of the North Atlantic seafloor from the southern tip of the Reykjanes Ridge at 50°N to the North Pole is shown in Figure 1, while ridge depths and cumulative lengths are listed in Table 1. The topography of the Reykjanes Ridge south of Iceland drops from subaeriel at Reykjanes Peninsula to a depth of about 1 km below sea level over about the first one third of the extent of the ridge and deepens further to almost 4 km over the remaining 1000 km of ridge. By contrast, the Kolbeinsey Ridge north of Iceland up to the Jan Mayen Island is quite shallow. North of Jan Mayen, the overall direction of the equally rather shallow Mohns Ridge is at a small angle to spreading, while further north yet, the Knipovich Ridge returns to more normal depths and an overall north-south trending direction.

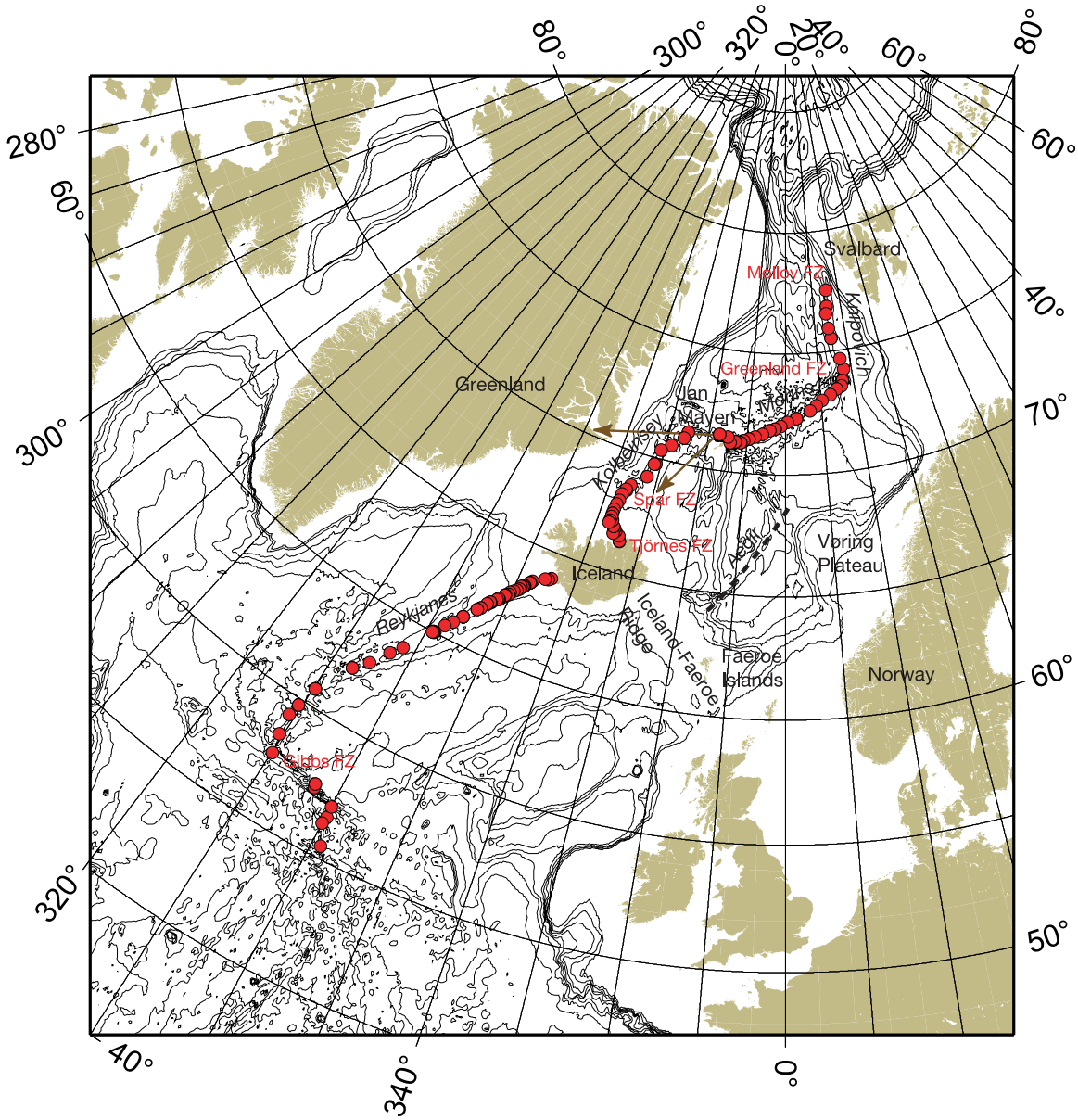

Figure 1. Map of the North Atlantic region showing locations of the dredged MORB glasses (red circles) analyzed in this study, as well as individual ridge segments, fracture zones, bathymetry contours (thin black lines), and other relevant tectonic features. The two arrows pointing in the directions of Greenland and Iceland from Jan Mayen show the trace of the European lithospheric movement over the hot spot reference frame during the past 25 Myr using the poles and velocities of *Gripp and Gordon* [2002] and the direction of the Jan Mayen Ridge.

[9] The nagging issue of the nature of the Jan Mayen Island continues to confuse the debate over the geodynamic evolution of the North Atlantic region. *Neumann and Schilling* [1984] and *Schilling et al.* [1999], among others, suggested that Jan Mayen is a hot spot volcano. In contrast, the seismic velocity structure under the Jan Mayen Ridge, a shallow promontory prolonging the island to the south, and under the Jan Mayen Basin, between the Kolbeinsey and the Jan Mayen Ridges, has been interpreted as indicating the presence of continental rocks [*Johnson and Heezen*, 1967; *Kodaira et al.*, 1998]. *Haase et al.* [1996] argued that the enrichment of the mantle beneath Jan Mayen in incompatible elements is best explained by it being wet and cold, characteristics these authors ascribed to the influence of the Greenland continental lithosphere on the Kolbeinsey Ridge.

[10] The nature of mantle components and ridge segmentation around Iceland, as well as entrainment of the mid-ocean ridge basalt (MORB) source

Table 1 (Representative Sample). Hf, Nd, and Pb Isotope Compositions and Lu/Hf Ratios of Mid-Atlantic Ridge Basalt Glasses From 50°N to 78°N, Including the Reykjanes, Kolbeinsey, Mohns, and Knipovich Ridges and the Jan Mayen Platform[a] [The full Table 1 is available in the HTML version of this article at http://www.g-cubed.org.]

Sample	Latitude, °N	Longitude, °W	Depth, m	Cumulative Distance,[b] km	Lu, ppm	Hf, ppm	$^{176}Lu/^{177}Hf$	$^{176}Hf/^{177}Hf \pm 2\sigma$	ε_{Hf}	$^{143}Nd/^{144}Nd \pm 2\sigma$	ε_{Nd}[c]	$^{206}Pb/^{204}Pb$	$^{207}Pb/^{204}Pb$	$^{208}Pb/^{204}Pb$
Knipovich Ridge														
EN026 25D-2g	77.53	7.67	2925	0	0.360	2.48	0.0206	0.283359 ± 10	20.76		9.30	18.2109	15.4444	37.8798
								0.283370 ± 06	21.15					
EN026 22D-1g	76.86	7.37	3450	75	0.436	2.71	0.0228	0.283382 ± 07	21.57		9.42	18.2731	15.4602	37.9720
								0.283389 ± 07	21.82			18.2688	15.4567	37.9645
EN026 21D-1g	76.56	7.19	2810	109	0.455	2.77	0.0233	0.283401 ± 07	22.24		10.03	18.1740	15.4338	37.8208
EN026 19D-1g	75.96	7.28	3258	175	0.433	2.89	0.0213	0.283388 ± 05	21.78		9.62	18.3044	15.4697	38.0473
EN026 27D-1	75.52	7.50	2600	224	0.470	2.87	0.0232	0.283331 ± 06	19.77		7.18	18.5476	15.5264	38.3904
												18.5536	15.5341	38.4166
												18.5524	15.5314	38.4089
EN026 27D-2	75.52	7.50	2600	224	0.437	2.88	0.0215					18.5509	15.5309	38.4016
EN026 29D-1g	74.65	8.51	2878	321	0.442	2.57	0.0244	0.283399 ± 05	22.17		9.89	18.1130	15.4392	37.8047
EN026 30D-1g	74.19	8.84	3210	373	0.401	2.56	0.0222	0.283382 ± 07	21.57		7.88	18.3409	15.4901	38.1472
EN026 31D-1g	73.74	8.37	3290	422	0.495	2.60	0.0270	0.283415 ± 09	22.74		9.71	18.0784	15.4355	37.7671
								0.283408 ± 06	22.49					
								0.283410 ± 10	22.49					
Mohns Ridge														
EN026 32D-3g	73.52	8.11	2288	447	0.398	2.01	0.0281	0.283401 ± 10	22.24		8.68			
EN026 16D-1g	73.41	7.39	2623	472	0.434	1.84	0.0335	0.283454 ± 07	24.12		9.11	17.9589	15.4345	37.6295
								0.283458 ± 08	24.26					
EN026 16D-2g	73.41	7.39	2623	472	0.390	1.87	0.0296	0.283448 ± 09[d]	23.91		10.26	17.9365	15.4262	37.6011
EN026 15D-1g	73.22	6.44	2840	509	0.398	2.01	0.0281	0.283318 ± 07	19.31		7.71			
TR139 33D-2g	73.01	5.18	2900	556	0.400	2.09	0.0272	0.283332 ± 06	19.80		7.61	18.2893	15.4616	38.0320
EN026 14D-1g	72.81	4.26	2540	594	0.442	2.12	0.0296	0.283431 ± 05	23.30		9.62	17.9114	15.4183	37.5932
TR139 32D-1Ag	72.61	3.38	3020	630	0.363	2.06	0.0250	0.283385 ± 12	21.68		8.23	18.2213	15.4501	37.9452
EN026 12D-2g	72.32	1.48	2525	702	0.373	2.61	0.0203	0.283300 ± 08	18.67		7.32	18.4967	15.4724	38.2634
EN026 12D-3g	72.32	1.48	2525	702	0.337	2.17	0.0220					18.4489	15.4571	38.1833
												18.4618	15.4650	38.2153
												18.4603	15.4654	38.2127
TR139 31D-2Ag	72.18	0.23	2462	747	0.461	2.23	0.0293	0.283409 ± 07	22.53		8.70	17.9917	15.4265	37.7069
EN026 11D-1g	71.99	−0.65	2340	783	0.428	2.57	0.0236	0.283338 ± 06	20.02		7.04	18.3717	15.4580	38.1091

[a] Lu and Hf concentrations measured by ICP-MS at URI. Hf and Nd isotope compositions analyzed by MC-ICP-MS (VG Plasma 54) at ENSL. $^{176}Hf/^{177}Hf$ and $^{143}Nd/^{144}Nd$ normalized for mass fractionation relative to $^{179}Hf/^{177}Hf = 0.7325$ and $^{146}Nd/^{144}Nd = 0.7219$, respectively. $^{176}Hf/^{177}Hf$ of JMC-475 Hf standard = 0.282160 ± 0.000010 and $^{143}Nd/^{144}Nd$ of La Jolla Nd standard = 0.511858 ± 0.000018 (both 2 sigma). Hf and Nd standards run every second sample. Uncertainties reported on Hf and Nd measured isotope ratios are in-run $2\sigma/\sqrt{n}$ analytical errors in last two decimal places, where n is the number of measured isotopic ratios. Pb isotope compositions analyzed by MC-ICP-MS (VG Plasma 54) at ENSL using the T1 doping technique. The external reproducibilities of $^{206}Pb/^{204}Pb$, $^{207}Pb/^{204}Pb$, and $^{208}Pb/^{204}Pb$ are 300, 350, and 430 ppm, respectively.

[b] Cumulative distance is distance along the ridge axis from the northernmost station (EN026 25D), ignoring fracture zone offsets.

[c] Nd isotope compositions given as ε_{Nd} only are from *Schilling et al.* [1999] and listed here for convenience.

[d] Hf isotope data from *Andres et al.* [2004]. Listed here for completeness and convenience.

Geochemistry Geophysics Geosystems G3
BLICHERT-TOFT ET AL.: RIDGE–HOT SPOT INTERACTION 10.1029/2004GC000788

by the Icelandic plume, represent additional insufficiently understood problems in this region. *Thirlwall* [1995] argued that Pb isotopes in Iceland basalts and MORB south of Iceland form parallel trends in a $^{208}Pb/^{204}Pb$ versus $^{207}Pb/^{204}Pb$ diagram and ascribed this to recent addition of U to the Iceland mantle source. *Hanan and Schilling* [1997] also argued for dual sources for the Reykjanes Ridge and Peninsula on the one hand and for the rest of Iceland on the other hand. In contrast, Mertz and coauthors [*Mertz et al.*, 1991; *Mertz and Haase*, 1997] could not confirm this dichotomy and contended that Iceland Pb overlaps with that of the neighboring ridges.

[11] Although a wealth of radiogenic isotope data is already available for the Reykjanes, Kolbeinsey, Mohns, and Knipovich Ridges and the Jan Mayen Platform [*Schilling et al.*, 1983; *Neumann and Schilling*, 1984; *Waggoner*, 1990; *Mertz et al.*, 1991; *Mertz and Haase*, 1997; *Schilling et al.*, 1999; *Trønnes et al.*, 1999], Hf isotope data and Pb isotope measurements of modern state-of-the-art precision were so far largely missing despite the significant potential of both of these sort of data. For example, decoupling of Hf from Nd isotope compositions is both uncommon and informative of the mantle source mineralogy, in particular the respective roles of garnet and clinopyroxene during MORB mantle melting [e.g., *Salters and Hart*, 1989; *Salters*, 1996; *Salters and White*, 1998; *Chauvel and Blichert-Toft*, 2001]. This stems from the fact that Lu is far more compatible in the presence of garnet than Sm. In addition, the dynamic range of $^{176}Hf/^{177}Hf$ in MORB is substantially greater than that of $^{143}Nd/^{144}Nd$, which arises because Lu/Hf is fractionated by melting much more so than Sm/Nd, such that a given degree of especially ancient melting will result in a more pronounced signal in Hf than Nd isotopic composition. This effect is accentuated by the half-life of ^{176}Lu being about three times shorter than that of ^{147}Sm, resulting in more rapid ingrowth of radiogenic ^{176}Hf than ^{143}Nd. As for the potential worth of high-precision Pb isotopes, the recent application of both triple-spike thermal ionization mass spectrometry (TIMS) [*Abouchami et al.*, 2000; *Eisele et al.*, 2003] and multicollector inductively coupled plasma mass spectrometry (MC-ICP-MS) [*Blichert-Toft et al.*, 2003] to Pb isotope analysis of basalts has revealed that much of the scatter previously observed in Pb isotopic data can be ascribed to analytical uncertainties in conventional TIMS measurements and have unveiled unexpectedly simple relationships between mantle geochemical components.

[12] To fill in the gap in the database for the North Atlantic province and to attempt to answer still pending questions from previous studies, the present work reports new Hf (and, where lacking from the literature, also Nd) and high-precision Pb isotope data, as well as Lu/Hf ratios, of MORB samples previously analyzed for major and trace elements and multiple other isotopes from the ~1700 km long segment of the MAR in the Arctic region that stretches northward from the Kolbeinsey Ridge at 66°N just north of Iceland over the Mohns Ridge to the Knipovich Ridge at 78°N. Although the main focus of this study is on these Arctic ridges, we also report Hf, Nd, and Pb isotope data and Lu/Hf ratios for MORB from the entire latitudinal extent of the ~1700 km long Reykjanes Ridge from 50°N to 64°N in order to reassess the interaction of the Iceland hot spot with both its northern and southern neighboring ridges. Some of the more detailed questions left unanswered by earlier investigations and to be readdressed here are (1) whether the Iceland plume-ridge interaction is symmetric or asymmetric about Iceland, (2) whether two or three components are involved in the plume-ridge mixing process, (3) whether the northern MAR is affected by one or two mantle plumes, Iceland and Jan Mayen, and, if the latter, whether they are isotopically distinguishable, (4) whether Jan Mayen is in fact a mantle plume or rather a piece of leftover continent, and if the former, what are the characteristics of the Jan Mayen plume-ridge interaction (5) whether the young, thermally immature Knipovich Ridge, and possibly also the Mohns Ridge, are affected by continental-derived material from the nearby Greenland craton. Furthermore, the Hf isotope data raise new questions regarding the nature of the upper mantle north of Jan Mayen and the role of continental crust versus garnet fractionation in producing MORB with ultra-depleted Hf isotopes that are unmatched by a similar depletion in Nd isotopes. Meanwhile, the high-precision Pb isotope data highlight the existence of major geochemical and convective mantle discontinuities along the Arctic MAR and thereby revive an old controversy about the contrasting behavior of Pb isotopes with respect to the other long-lived radiogenic isotope systems. The ensuing discussion focuses on the large-scale implications of these data for mantle components and overall structure beneath the North Atlantic and the possible, much disputed geodynamic significance

of the Jan Mayen Island and Ridge. A summary of the abundant previous work done on the Arctic MAR is provided for background information in Appendix A.

2. Tectonic Setting of the Arctic MAR

[13] A general notion of the broad tectonic setting of the study area can be gained from Figure 1. Ridge elevation along the Arctic MAR north of Iceland decreases gradually from sub-aerial over Iceland and the Tjörnes Transform Zone to a maximum depth of about 3.5 km over the Knipovich Ridge (Table 1). Simultaneously, the half spreading rate and the mean degree of melting along this part of the Arctic MAR decrease from, respectively, 1 to 0.6 cm/yr and by a factor of 2 to 3 [*Schilling et al.*, 1999]. While the spreading rate gradually winds down over the Arctic MAR to a near halt under the polar ice cap, tectonic and thermal conditions become increasingly extreme.

[14] The mature Kolbeinsey Ridge north of Iceland up to the Jan Mayen Island is quite shallow (Table 1), probably due to its proximity to the Iceland mantle plume. It is bound by the Jan Mayen Fracture Zone to the north and the Tjörnes Transform Zone to the south and is intersected about halfway through by the Spar Fracture Zone separating southern Kolbeinsey from northern Kolbeinsey Ridge. The southern Kolbeinsey Ridge axis has a crest-like morphology up to the Spar Fracture Zone, after which a small rift develops further north. North of Jan Mayen, the overall direction of the also fairly shallow Mohns Ridge (Table 1), which is confined between the Jan Mayen Fracture Zone and the now extinct Greenland Fracture Zone, is at a small angle to spreading, which explains the en-echelon morphology of this accreting boundary [*Géli et al.*, 1994]. It has a well-developed rift except over the Jan Mayen Platform, where its exact location is poorly known. Further north still, the immature and slow-spreading Knipovich Ridge, which is located on the fringe of the Barents Sea-Svalbard continental platform, is oriented essentially parallel to the Baltic continental shelf break, and extends from the Greenland Fracture Zone to the complex Molloy Transform Zone. Relative to the preceding ridge segments, this section of the MAR is characterized by more normal ridge depths on the order of about 3 km below sea level (Table 1). The Knipovich Ridge makes a sharp change of course to the northwest relative to the Mohns Ridge, thus returning to a direction near-perpendicular to latitude. Its ridge axis is discontinuous, often graben-like, heavily sedimented by turbidites, and dominated by a punctiform nature of volcanism. Spreading is highly oblique, nearly shear-like and either the present position of the Knipovich axis resulted from a relatively recent rift jump within this only 35 Ma old basin or the spreading is highly asymmetrical. In contrast, the Mohns Ridge has spread symmetrically and remained in its present position for the last 40–60 Ma, which is essentially since this part of the Atlantic formed. The Kolbeinsey Ridge has been in its present position for at least 10 Ma, its ancestor being the Aegir Ridge [*Jung and Vogt*, 1997]. The Mohns and Kolbeinsey Ridges are separated by the Jan Mayen Ridge or Platform, which may be either a splinter of continental lithosphere left over from the complex opening of the Atlantic basin [e.g., *Nunns*, 1983; *Myhre et al.*, 1984; *Skogseid and Eldholm*, 1987] or the possible locus of another hot spot separate from that under Iceland [e.g., *Schilling et al.*, 1999].

3. Samples

3.1. Arctic MAR North of Iceland

[15] Hafnium and Pb isotope data for the Arctic ridges were acquired on a subset of about 60 Arctic MAR basalt glasses from 66–78°N, covering the Kolbeinsey (66–71°N), Mohns (71.5–73.5°N), and Knipovich (73.5–78°N) Ridges, the Tjörnes Transform Zone (66–67°N), the Spar Fracture Zone (69°N), and the Jan Mayen Platform (71–72°N) (Figure 1). The sampling of the Tjörnes Transform Zone includes basalts from the Kolbeinsey Rock, Grimsey Island, and the two Manareyjar islets of Lagey and Hauy. All the samples are the same fresh MORB glasses (and interiors in the case of subaerial basalts) that were previously analyzed for major and trace elements, and Sr, Nd, conventional Pb, and He isotopes [*Schilling et al.*, 1983, 1999; *Neumann and Schilling*, 1984; *Waggoner*, 1990] and are part of the University of Rhode Island (URI) dredge rock collection. The new isotope data presented here can therefore, and will be, directly integrated with the existing chemical and isotopic data sets of previous URI investigations (which consist of both published and unpublished data). To complement our Hf isotope data, we also measured the Nd isotope compositions for five samples from Jan Mayen, which had not been previously analyzed by *Schilling et al.* [1999], but that we had included in this study to better define Jan Mayen isotopically with respect to Iceland. Finally, we measured the Lu and Hf concentrations

for the samples analyzed for Hf isotopes, since these data were lacking from the existing URI trace element database and bear directly on the Hf isotope data.

3.2. Reykjanes Ridge South of Iceland

[16] Hafnium, Nd, and Pb isotope data and Lu and Hf concentrations were also acquired for about 60 MORB glasses from the Reykjanes Ridge and Peninsula (50–64°N), including the Gibbs Fracture Zone (52.5°N). All samples were retrieved from the URI dredge rock collection.

4. Analytical Techniques

[17] Hafnium for isotope analysis was separated from clean, handpicked glass chips at either the Ecole Normale Supérieure in Lyon (ENSL) or URI following the procedure described in *Blichert-Toft et al.* [1997]. The isotopic compositions of the Hf separates were measured by MC-ICP-MS at ENSL using its VG Plasma 54 and the technique of *Blichert-Toft et al.* [1997]. In order to monitor machine performance, the JMC-475 Hf standard was run systematically after every two samples and gave, throughout this study, 0.282160 ± 0.000010 (2 sigma) for $^{176}Hf/^{177}Hf$, corresponding to an external reproducibility of 35 ppm (0.35ε). Five samples were analyzed in duplicate and one sample in triplicate. One of these (TR139 20D-1g) was chosen for repeat measurement because of an in-run error significantly greater than the external reproducibility during its first run (Table 1), whereas the other five samples were selected for replication in order to verify their unexpectedly radiogenic Hf isotope compositions. The excellent reproducibility within external error of all replicate analyses (Table 1) and the consistency of Hf isotope compositions between geographically neighboring samples (analyzed in random sequence) indicate that our error assignment is conservative. Hafnium total procedural blanks were less than 25 pg for all sample batches.

[18] For the five samples that were also measured for their Nd isotope compositions, the analyses were done at ENSL on the same sample dissolutions as those used for the Hf (and Pb) isotope work. An aliquot of the redissolved fluoride precipitate left over from the first step of the Hf separation chemistry was passed through a cation exchange column to separate the rare earth element (REE) fraction, which in turn was run through an HDEHP column to isolate the Nd. The Nd isotope compositions were measured on the Plasma 54 using the same routine as for Hf isotope measurement, signifying that machine performance was monitored by analyzing the La Jolla Nd standard after every second sample. It gave 0.511858 ± 0.000018 (2 sigma) for $^{143}Nd/^{144}Nd$, corresponding to an external reproducibility of 35 ppm (0.35ε). Neodymium total procedural blanks were less than 200 pg.

[19] Lead for isotope analysis was separated at ENSL. The handpicked glass chips were first leached for a total of 50 min in distilled 6 M HCl, including both heating steps on a hot plate and ultrasonication. Lead was subsequently separated on 50 μl anion-exchange microcolumns using 0.5 M HBr to elute the sample matrix and 6 M HCl to recover the Pb. In order to ensure efficient and clean Pb separation for optimization of mass spectrometer operation, the Pb fraction was run twice through the anion-exchange column. Lead yields were checked to be ~100%, thus eliminating the effect of Pb fractionation on the column [*Blichert-Toft et al.*, 2003]. Lead isotope compositions were measured on the Plasma 54 as described by *White et al.* [2000] using added normal Tl to correct for instrumental mass fractionation. Machine performance was monitored by analyzing the NBS-981 Pb standard every two samples, to which the samples were subsequently normalized by interpolation using the values by *Todt et al.* [1996]. The interpolation was done such that the standard closest to a given sample was weighted by two thirds, while the standard farthest from the sample was weighted by one third. Measurement accuracy was verified by repeatedly measuring an in-house Pb standard mixture (ENSL-98B, which is a mixture of the NBS Pb standards 981 and 982). The Pb isotope ratios obtained for this standard mixture during the period of acquisition of the present Arctic MAR Pb isotope data are compiled in Figure 2 and demonstrate an external reproducibility of 300, 350, and 430 ppm, respectively, for $^{206}Pb/^{204}Pb$, $^{207}Pb/^{204}Pb$, and $^{208}Pb/^{204}Pb$ on about 50 analyses of ENSL-98B. By contrast, the Pb isotope ratios not involving the less abundant ^{204}Pb isotope, $^{207}Pb/^{206}Pb$ and $^{208}Pb/^{206}Pb$, both have an external reproducibility better than 50 ppm. Four duplicate and two triplicate Pb analyses of our Arctic samples (Table 1) fall well within these error bars except for $^{207}Pb/^{204}Pb$ of sample TR139 9D-2A, which shows a 550 ppm difference between the two analyses. We ascribe this deviancy to the fact that only very little sample was left for this particular replicate measurement, resulting in a

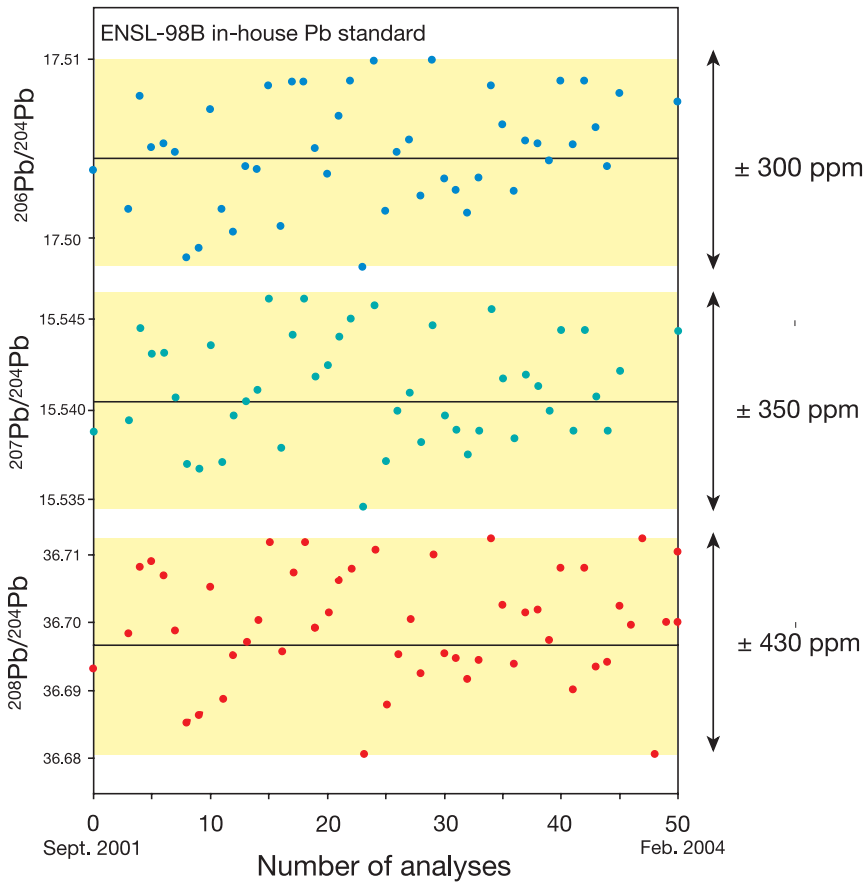

Figure 2. Values of $^{206}Pb/^{204}Pb$, $^{207}Pb/^{204}Pb$, and $^{208}Pb/^{204}Pb$ of about 50 analyses of the ENSL Pb in-house standard 98B (a mixture of NBS 981 and 982) as run on the ENSL Plasma 54 during the period from September 2001 to February 2004 and showing an external reproducibility of about 300–400 ppm. The external reproducibilities of $^{207}Pb/^{206}Pb$ and $^{208}Pb/^{206}Pb$ are better than 50 ppm.

marginally sized Pb ion beam and thus relatively poorer precision. Lead total procedural blanks consistently were less than 40 pg for all sample batches.

[20] Most of the Hf, Nd, and Pb isotope work for the samples from the Reykjanes Ridge were undertaken after completion of the Arctic samples. The same procedures as described above for the Arctic samples were followed except that now all three elements were systematically separated in cascade from the same sample dissolution. Exceptions are three samples in Table 1, one of which is lacking Nd (TR101 19D-1) and the other two Hf (TR101 3D-1g and GLJ 7g) isotope compositions, but not Pb. For these samples, the Hf or Nd had already been analyzed separately before commencement of the present project, which originally was focused on Pb, and we unfortunately failed to systematically catch and produce all the missing Hf and Nd isotope compositions simultaneously with the Pb isotope analyses before sample material had been exhausted by the latter. The one sample from Reykjanes Ridge that has Nd and Hf, but no Pb isotope data (TR138 11D-1g), had been analyzed for the former two and expended from the rock collection prior to initiation of the Pb work.

[21] It has been argued that MC-ICP-MS may produce Pb isotope results erroneous by up to 400 ppm per atomic mass unit [*Thirlwall*, 2002], which *Albarède et al.* [2004] showed to be a probable outcome of the large residual background of some instruments. Recently, *Baker et al.* [2004] claimed that the $^{207}Pb/^{204}Pb$ of the Theistareykir (Iceland) subaerial basalts measured by *Stracke et al.* [2003] on the ENSL Plasma 54 is too low by up to 3 per mil compared to the double-spike results acquired on the same lava flows by this group. We have shown [*Albarède et al.*, 2005], however, that Pb isotopic analyses

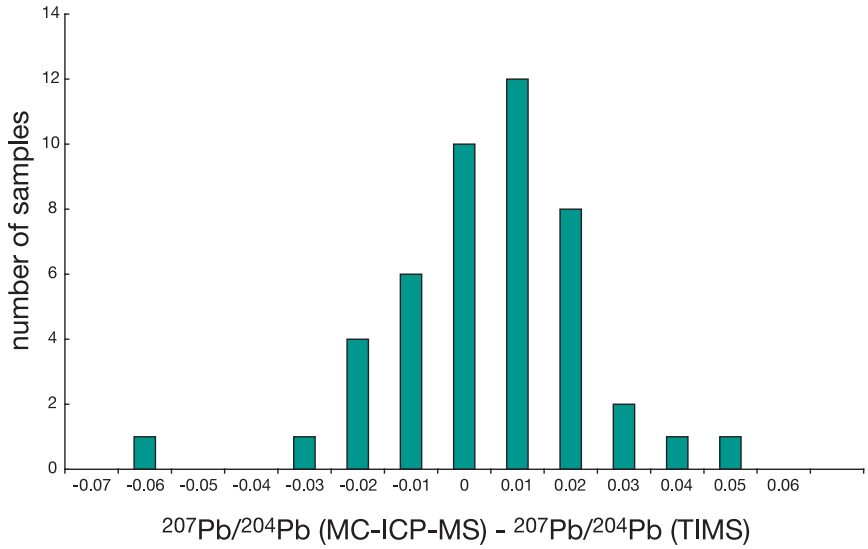

Figure 3. Histogram showing a comparison between $^{207}Pb/^{204}Pb$ for TIMS and MC-ICP-MS data for all the submarine samples analyzed in the present work. The two methods display an agreement of 0.03 at the 95% confidence level.

are very sensitive to leaching procedures, especially, as previously identified for Hawaiian basalts by *Eisele et al.* [2003], when subaerial volcanics contaminated by meteoric water and aerosols are measured. Using TIMS and triple-spike, these authors showed that different dissolutions of subaerial samples leached to variable extents produce $^{207}Pb/^{204}Pb$ ratios different by up to 500 ppm, whereas the results are reproducible within external error bars for submarine samples. *Stracke* [2001] made a similar observation and found that the $^{207}Pb/^{204}Pb$ of unleached samples in the Theistareykir lava flows obtained by MC-ICP-MS and TIMS were consistent, but substantially more radiogenic than the leached samples, the values of which were those to be ultimately published by *Stracke et al.* [2003]. Figure 3 confirms that, in the present case, our submarine samples are free from this problem: a comparison of $^{207}Pb/^{204}Pb$ shows an agreement of 0.03 at the 95% confidence level between TIMS [*Schilling et al.*, 1999] and MC-ICP-MS data. The histogram of the deviations for each sample is symmetrical, which clears the suspicion of a systematic bias of one method over the other. We assert that most of the variance between the two data sets is a result of the mass bias fluctuations inherent to TIMS analysis and is fully consistent with the errors quoted in the original publication [*Schilling et al.*, 1999]. With the exception of one sample, EN026 16D-1g, which is identified as an outlier in the TIMS, but not in the MC-ICP-MS data set when viewed as a function of latitudinal variation (not shown), the new high-precision Pb isotope data measured here by MC-ICP-MS thus correlate remarkably well with the TIMS Pb isotope data published for the same samples by *Schilling et al.* [1999]. This is further illustrated in Figure 4, where MC-ICP-MS Pb plots on a well-defined 1:1 correlation line with respect to TIMS Pb for all three Pb isotope ratios. This relationship mutually endorses both Pb isotope data sets.

[22] Lu and Hf concentrations were analyzed by internal and external standardization using a high-resolution, inductively coupled plasma mass spectrometer (HR-ICP-MS) at URI. Precision for Lu and Hf are estimated at 1.7% and 2.5% relative standard deviation, respectively, on the basis of multiple runs (n = 42) of an in-house standard MORB from the Mohns Ridge (EN026 10D-3). Accuracy of the method is estimated by comparing the average value of seven runs of separate USGS basalt standards (BHVO-1, BIR-1, and BCR-1), analyzed concurrently with the samples from this study, with accepted values [*Govindaraju*, 1994; W. F. McDonough, personal communication, 1994], as listed in Table 2.

5. Results

[23] The Hf, Nd, and Pb isotope data and Lu and Hf concentrations (also given as $^{176}Lu/^{177}Hf$ using

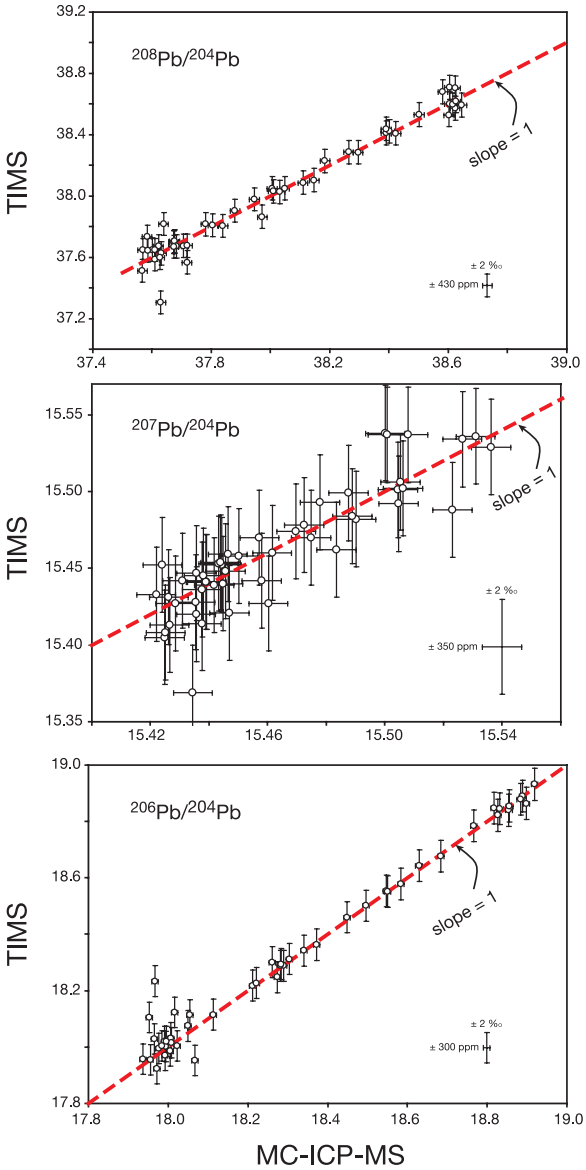

Figure 4. Values of $^{206}Pb/^{204}Pb$, $^{207}Pb/^{204}Pb$, and $^{208}Pb/^{204}Pb$ measured by TIMS [*Schilling et al.*, 1999] versus $^{206}Pb/^{204}Pb$, $^{207}Pb/^{204}Pb$, and $^{208}Pb/^{204}Pb$ measured by MC-ICP-MS (this study). With the exception of one sample, which is a TIMS outlier, all three Pb isotope ratios show a good 1:1 correlation between the two methods.

0.1419 as conversion factor) are listed in Table 1. The Nd isotope data reported in this table as ε_{Nd} only are those previously published by *Schilling et al.* [1999] and have been included here for convenience. In all consecutive plots for which geographical location (i.e., latitude) is a key parameter, we chose for simplicity and better readability, as well as to preserve a more direct perception of the data on plots, to present them as a function of latitude rather than radial distance from the Euler pole or cumulative distance (which is nevertheless listed in Table 1 for reference). When plotting the latitude with respect to the rotation pole versus the geographical latitude (not shown), the relationship is nearly linear. Thus using either one of these parameters as plotting variable makes little difference to the fundamental data display. The slight overlap in latitude of northern Kolbeinsey Ridge with the Jan Mayen Platform and the southern tip of Mohns Ridge (Figure 1, Table 1) and the fact that Mohns Ridge does not run perpendicular to latitude, but is more east-west trending (Figure 1), simply has the effect of somewhat compressing this subset of data on the latitudinal variation plots, but does not alter its relative position or pattern with respect to the data subsets from the other ridge segments.

5.1. Hf-Nd Isotope Systematics

[24] The Hf and Nd isotopic variations along the ridges are presented in Figure 5, while Figure 6 shows a plot of ε_{Hf} versus ε_{Nd}, which includes literature data on Iceland for reference [*Kempton et al.*, 2000; *Stracke et al.*, 2003; *Malfère*, 2004].

[25] On the southern Kolbeinsey Ridge (Figure 5), ε_{Hf} and ε_{Nd} increase steeply in a northerly direction until reaching a plateau which extends over several degrees of latitude and where typical N-MORB erupt. This gradient is usually interpreted to reflect mixing of the Iceland plume with depleted upper mantle. A similar pattern, but in mirror image and much less steep, is observed in a southerly direction along the Reykjanes Ridge south of Iceland, where ε_{Hf} and ε_{Nd} gradually increase with distance away from Iceland. This gradient likewise is believed to reflect simple plume-ridge interaction. The unradiogenic Hf-Nd component, which probably originates within the Iceland plume itself, is present both north and south of Iceland and the

Table 2. Average Lu and Hf Concentration Values of USGS Basalt Standards Analyzed Simultaneously With the Samples From This Study, Compared With Certified Values

USGS Standards	Lu	Hf
BIR-1 (n = 7)	0.248	0.59
Certified	0.253	0.58
BHVO-1 (n = 7)	0.284	4.57
Certified	0.278	4.30
BCR-1 (n = 7)	0.501	5.07
Certified	0.499	4.97

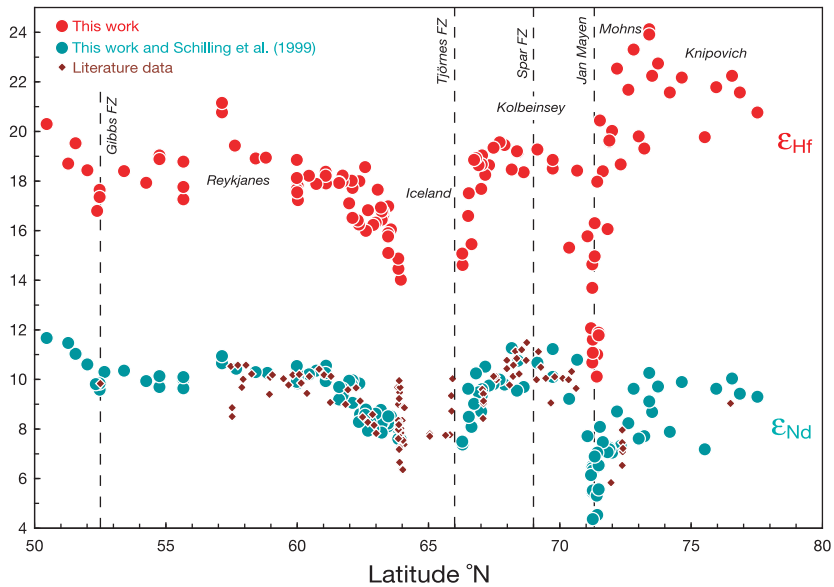

Figure 5. Values of ε_{Hf} and ε_{Nd} versus latitude for North Atlantic MORB. Note the regional decoupling between Hf and Nd isotopes, which is most easily seen from the relative magnitudes of the maxima where N-MORB erupt. The ε_{Hf} maximum of +24 over Mohns Ridge is significantly higher than that of +19 over Kolbeinsey Ridge, whereas the opposite is observed for ε_{Nd}. The anomaly clearly is over Mohns Ridge, not the Kolbeinsey Ridge, and the anomalous isotopes are those of Hf, not Nd. Note the good agreement between the Nd isotope data of this study and data from the literature. Literature Nd isotope data are from *Mertz et al.* [1991], *Mertz and Haase* [1997], *Schilling et al.* [1999], and *Thirlwall et al.* [2004].

halo polluted by Hf and Nd is strongly asymmetrical extending over only one degree of latitude along the Kolbeinsey Ridge, but over five degrees of latitude along the Reykjanes Ridge.

[26] On the northern Kolbeinsey Ridge (Figure 5), ε_{Hf} and ε_{Nd} decrease, again very steeply, toward Jan Mayen, presumably showing mixing between depleted upper mantle and the Jan Mayen plume (assuming Jan Mayen is a hot spot). The Spar Fracture Zone seems to separate MORB affected by the Iceland plume on the southern Kolbeinsey Ridge from those affected by the Jan Mayen plume on the northern Kolbeinsey Ridge. The samples from the Jan Mayen Platform (north of the island) display by far the most unradiogenic Hf and Nd isotope compositions on this section of the Arctic MAR, including Iceland, thus suggesting that the Arctic MAR is indeed affected by two isotopically distinct mantle plumes, i.e., those beneath Iceland and Jan Mayen. Along Reykjanes, Kolbeinsey, and Jan Mayen, Hf and Nd isotopes vary in concert.

[27] In contrast, on the Mohns Ridge (Figure 5), ε_{Hf} increases abruptly and continuously, from +10 at the Jan Mayen Platform to more than +24 at the intersection of the northern tip of this ridge with the Knipovich Ridge, where N-MORB (normal MORB) erupt with ε_{Nd} of +10, which is rather unradiogenic in comparison with the high companion values of ε_{Hf}. The steep gradient in Hf isotope composition, which over Mohns Ridge never levels out such as over Kolbeinsey Ridge, extends at its highest value to more than five ε_{Hf} units above the level of the Kolbeinsey Ridge and is thought to reflect mixing of the Jan Mayen plume with ultra-depleted upper mantle, the nature of which will be discussed in more detail below.

[28] Finally, along the Knipovich Ridge (Figure 5), ε_{Hf} scatters between +20 and +23, which, as for the Mohns Ridge, is highly radiogenic, especially when compared to a range of between only +7 and +10 for ε_{Nd}. With the exception of a few isolated samples from the Australian-Antarctic Discordance [*Hanan et al.*, 2004] and the Azores (J. Blichert-Toft, unpublished data, 2004), the Mohns and Knipovich Ridge basalts display, for any given Nd isotope composition, the most consistently radiogenic Hf reported so far for any MORB worldwide [e.g., *Patchett and Tatsumoto*, 1980; *Salters and White*, 1998; *Chauvel and Blichert-Toft*, 2001]. In addition, this conspicuous, unusually radiogenic Hf signal is not confined to only a few samples, but is present

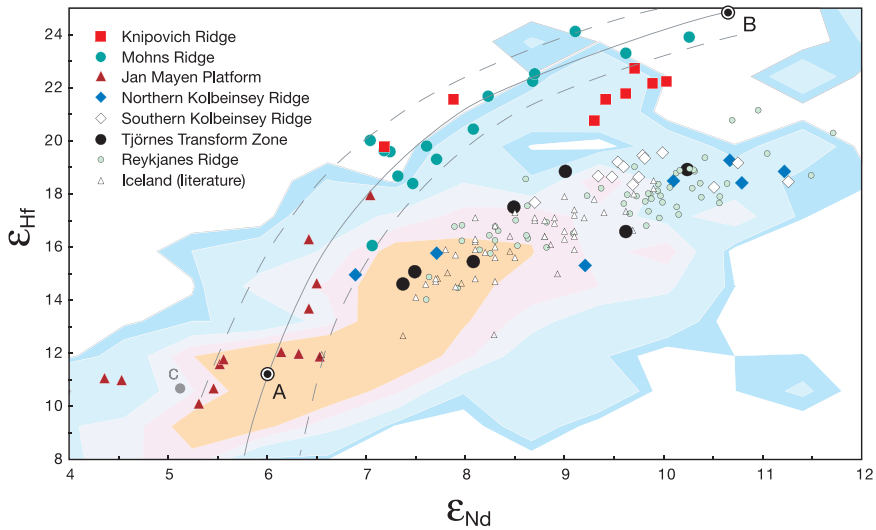

Figure 6. Values of ε_{Hf} versus ε_{Nd} for North Atlantic MORB with literature data for Iceland [*Kempton et al.*, 2000; *Stracke et al.*, 2003; *Malfère*, 2004] plotted for reference. The multicolored backdrop is a contouring of the mantle array based on ~2200 MORB and OIB of global distribution (J. Blichert-Toft, unpublished data, 2004, and literature data from references too numerous to all be cited here). The Kolbeinsey and Reykjanes samples, including the samples from the Tjörnes Fracture Zone, plot together with samples from Iceland in a well-correlated group that fall in the center of the mantle array and has significantly less radiogenic Hf than the Mohns and Knipovich basalts, which form a separate group characterized by far more radiogenic Hf for any given Nd isotope composition. The Jan Mayen samples fall at the most unradiogenic values for this region at the convergence between the two groups defined by the Reykjanes-Iceland-Kolbeinsey and the Mohns-Knipovich samples, respectively. The Mohns Ridge samples delineate a strongly curved hyperbolic array with the samples from Jan Mayen, and possibly also those from the Knipovich Ridge. The unradiogenic end-member, labeled A and potentially compatible with the so-called "C" (or FOZO or PHEM) component, is consistent with the isotopic composition of Jan Mayen, whereas the highly radiogenic end-member, labeled B, resembles nothing normally sampled by the MORB melting process. The downward concavity of the mixing hyperbola indicates that the radiogenic end-member has a higher Hf/Nd ratio than the unradiogenic end-member, thus excluding the involvement of pelagic sediment. Note that C is actually a region on this diagram rather than a single point as indicated here for simplicity with the gray solid circle which merely represents the mean of the ranges of ε_{Hf} (+7.2 to +14.3) and ε_{Nd} (+4.1 to +6.1) values for C. The unradiogenic end-member A thus falls well within the C region and close to its mean value.

persistently along almost 1000 kilometers of continuous ridge (Table 1) and thus represents a distinct mantle source.

[29] In contrast to the samples from Reykjanes, Kolbeinsey, and Jan Mayen, a distinct regional decoupling between Hf and Nd isotopes is observed for the samples from the Mohns and Knipovich Ridges and is evident from both Figures 5 and 6. In addition, scatter in the Hf and Nd isotope data is particularly strong over these two ridge segments, as has also been observed previously for other geochemical parameters [*Schilling et al.*, 1999]. The regional decoupling is most easily perceived from the relative levels of the magnitudes of the two latitudinal maxima where N-MORB erupt. The ε_{Hf} maximum of +24 over Mohns Ridge is significantly higher than that of +19 over the Kolbeinsey Ridge, whereas the exact opposite is observed for ε_{Nd}. The anomaly clearly is over the Mohns Ridge, not the Kolbeinsey Ridge, and is displayed by Hf isotopes, not Nd.

[30] The decoupling between Hf and Nd isotope systematics over the Mohns and Knipovich Ridge segments is also reflected in the corresponding parent/daughter ratios in that the $^{176}Lu/^{177}Hf$ latitudinal profile (not shown) resembles that of $^{143}Nd/^{144}Nd$ (and $^{147}Sm/^{144}Nd$) rather than that of $^{176}Hf/^{177}Hf$. This decoupling between parent/daughter-$^{176}Hf/^{177}Hf$ (but not parent/daughter-$^{143}Nd/^{144}Nd$) is readily discerned from Table 1, which shows overall sub-chondritic $^{176}Lu/^{177}Hf$ for the Mohns and Knipovich basalts, whereas most of the Kolbeinsey basalts, which are far less radiogenic in Hf than the Mohns-Knipovich samples, have overall super-chondritic $^{176}Lu/^{177}Hf$.

[31] In ε_{Hf}-ε_{Nd} space (Figure 6), the Kolbeinsey Ridge MORB, including those of the Tjörnes Fracture Zone, plot in or near the field of Icelandic basalts, as does the MORB from Reykjanes Ridge. Together these samples define a well-correlated group that fall within the mantle array and is characterized by significantly less radiogenic Hf for a given Nd isotope composition than the MORB from the Mohns and Knipovich Ridges, which form a completely separate group with much more radiogenic Hf for any given Nd isotope composition. The samples from Jan Mayen plot with the most unradiogenic values at the convergence of the Reykjanes-Iceland-Kolbeinsey and Mohns-Knipovich groups.

[32] The Mohns Ridge MORB define a strongly curved hyperbolic mixing array with the samples from the Jan Mayen Platform, and possibly also the samples from the Knipovich Ridge. The unradiogenic end-member of this mixing hyperbola is consistent with the average isotopic composition of the samples from Jan Mayen, while the radiogenic end-member is unusually radiogenic, with ε_{Hf} values of up to more than +24 and resembling nothing normally sampled by the processes accountable for the mantle array. In the only other MORB samples with such radiogenic Hf (from the Australian-Antarctic Discordance; *Hanan et al.*, 2004), the radiogenic Hf is accompanied by virtually equally radiogenic Nd, whereas the Arctic samples of this study differ by exhibiting the ultra-depleted isotopic signature particularly strongly for Hf.

5.2. Pb Isotope Systematics

[33] The Pb isotope variations with latitude are shown in Figure 7, while the isotopic Pb-Pb plots are shown in Figures 8 and 9. In plots involving the small ^{204}Pb isotope, most literature TIMS data, in particular those from subaerial Icelandic volcanoes, scatter too much to be useful and therefore have not been included here. In contrast, the present data form consistent relationships with previously published high-precision Pb isotope data from the Reykjanes Ridge [*Thirlwall et al.*, 2004] and the ridges north of Iceland [*Mertz et al.*, 1991; *Mertz and Haase*, 1997; *Thirlwall et al.*, 2004] (Figure 7). In a ^{207}Pb/^{204}Pb versus ^{206}Pb/^{204}Pb plot (Figure 8), most ridge samples define a single linear array with a few samples, notably from the Knipovich Ridge, plotting toward higher ^{207}Pb/^{204}Pb. In contrast, the Theistareykir data of *Stracke et al.* [2003] have significantly lower ^{207}Pb/^{204}Pb than North Atlantic MORB (Figure 8). In the ^{208}Pb/^{204}Pb versus ^{206}Pb/^{204}Pb plot (Figure 8), and, even more visibly, in the ^{208}Pb/^{206}Pb versus ^{207}Pb/^{206}Pb plot (Figure 9), which is much less prone to analytical mass bias and contamination effects than the ^{204}Pb plots of Figure 8, the contrast between MORB north and south of Iceland is very pronounced. The two trends connect through the most unradiogenic samples from Iceland, the Tjörnes Fracture Zone, and the Kolbeinsey Ridge. In the ^{208}Pb/^{206}Pb versus ^{207}Pb/^{206}Pb plot (Figure 9), in which all conventional TIMS data can be plotted with minimum scatter, the trend of decreasing ^{207}Pb/^{206}Pb northward along the Reykjanes Ridge reverts along the Reykjanes Peninsula [*Thirlwall et al.*, 2004] toward the much higher values characteristic of subaerial samples, including the Theistareykir data of *Stracke et al.* [2003] (Figure 9). This layout is reminiscent of that previously proposed on a much more local scale by *Thirlwall* [1995] and *Hanan and Schilling* [1997], but the improved quality of the more recent Pb isotope data now helps strengthen the case.

6. Discussion

[34] The present data do not shed further light on the issue of the origin of the Icelandic source material, which has been, and continues to be, debated at length in the literature [*Chauvel and Hémond*, 2000; *Hanan et al.*, 2000; *Kempton et al.*, 2000; *Stracke et al.*, 2003; *Thirlwall et al.*, 2004]. As stressed by *Mertz and Haase* [1997], however, the Sr, Nd, and Pb isotope geochemistry of MORB north of Iceland seems to overlap with that of Iceland itself and this, we here observe, is also the case for Hf (Figure 6). For Hf and Nd, the overlap of data for Iceland with data for the Tjörnes Fracture Zone and the Kolbeinsey Ridge is nearly complete. In contrast, although the Pb isotope data from the Tjörnes Fracture Zone and the southern Kolbeinsey Ridge overlap with the least radiogenic Iceland data (Figures 8 and 9), the Pb isotope compositions of subaerial Iceland lavas are clearly distinct from the MORB data north and south of the hot spot. At the same time, the present data highlight the contrast between the isotope compositions of Pb from MORB north (Kolbeinsey Ridge) and south (Reykjanes Ridge) of Iceland [*Mertz et al.*, 1991], which stands out particularly well in ^{208}Pb/^{206}Pb-^{207}Pb/^{206}Pb space (Figure 9) with Pb data from subaerial Iceland extending as a linear array across the gap. The Iceland plume therefore mixes with material from both north

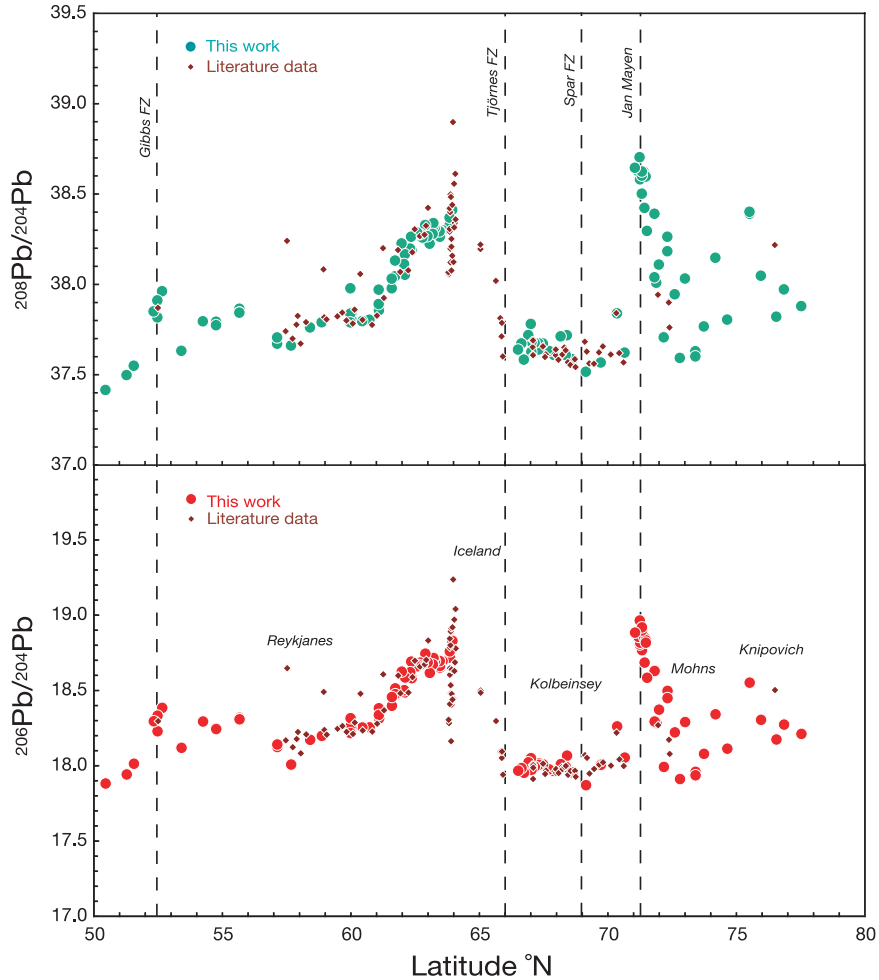

Figure 7. Values of $^{206}Pb/^{204}Pb$ and $^{208}Pb/^{204}Pb$ versus latitude for North Atlantic MORB. Note the distinct segmentation of the ridge by Iceland and Jan Mayen into three isotopically identifiable units. Note also the good agreement of the Pb isotope data of this study with data from the literature. Literature Pb isotope data are from *Mertz et al.* [1991], *Mertz and Haase* [1997], and *Thirlwall et al.* [2004].

and south of the hot spot. This reconciles *Thirlwall*'s [1995] and *Hanan and Schilling*'s [1997] claims that two separate trends exist around and within Iceland with *Mertz and Haase*'s [1997] assertion that the gap between these two trends simply reflects undersampling [see also *Malfère*, 2004].

6.1. Lead Principal Component Analysis

[35] As seen from Figures 5, 7, 8, and 9, the MORB mantle south of Iceland is extremely different from the MORB mantle north of Iceland, which in turn is very different from the MORB mantle north of the Jan Mayen Island. In order to substantiate this point, we processed through Principal Component Analysis (PCA) [e.g., *Albarède*, 1995] a set of some 180 high-precision Pb isotopic compositions consisting of the present data complemented by those of *Thirlwall et al.* [2004]. Mixing using ratios with a different denominator does not produce linear arrays and therefore the full isotopic data set is not amenable to PCA without a cost. In addition, partial melting fractionates elemental ratios and, as a result of different melt histories, a binary mixture in the source does not translate into a single hyperbola in the melts. The resulting deviations from linearity greatly increase dispersion in the multielemental space of isotopic compositions, often to the extent that spurious endmembers will appear. We are therefore not presenting PCA results on the bulk of the existing isotopic data, that is inclusive of Sr, Nd, and Hf isotope compositions, but only on the Pb isotope compo-

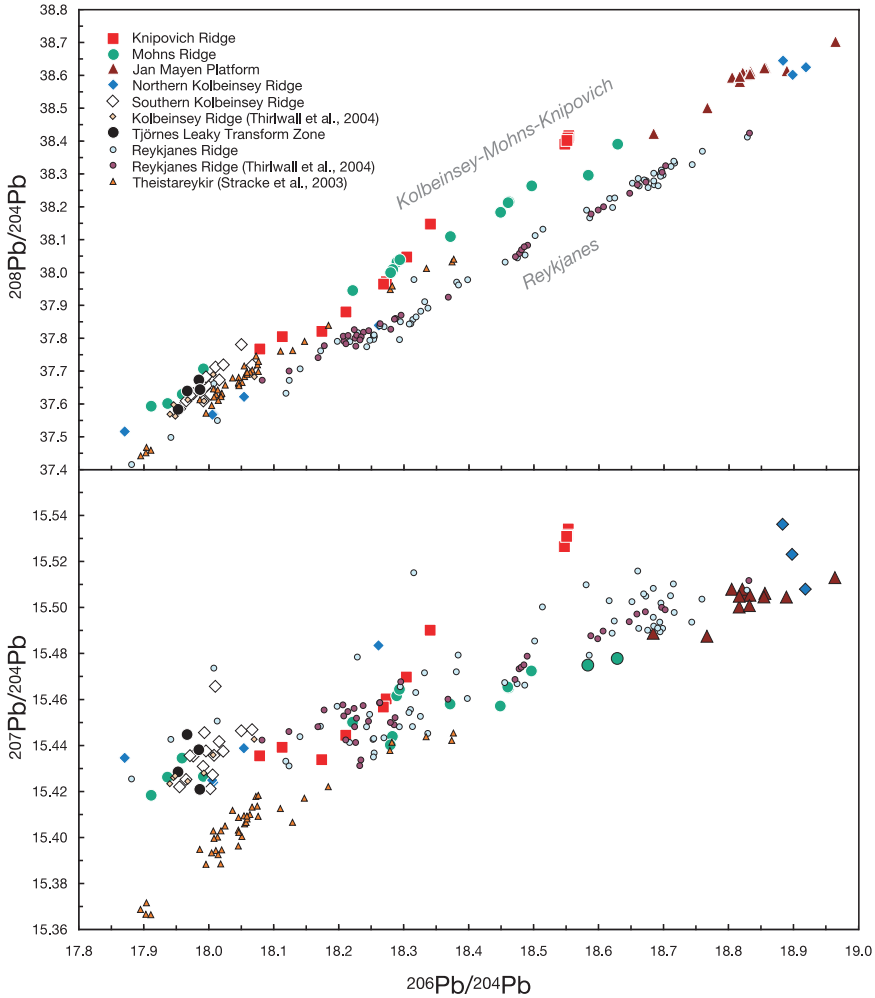

Figure 8. Values of $^{207}Pb/^{204}Pb$ and $^{208}Pb/^{204}Pb$ versus $^{206}Pb/^{204}Pb$ for North Atlantic MORB and Theistareykir (Iceland). In $^{207}Pb/^{204}Pb$-$^{206}Pb/^{204}Pb$ space, most of the North Atlantic ridge samples define a single linear array with the exception of a few samples, notably from the Knipovich Ridge, that exhibit higher $^{207}Pb/^{204}Pb$. In $^{208}Pb/^{204}Pb$-$^{206}Pb/^{204}Pb$ space, a pronounced difference between MORB north and south of Iceland stands out. The Theistareykir data of *Stracke et al.* [2003] have significantly lower $^{207}Pb/^{204}Pb$ than North Atlantic MORB. The conventional Pb isotope data of *Mertz et al.* [1991] and *Mertz and Haase* [1997] for North Atlantic MORB have not been included in these plots as they show too much scatter to be useful. Only the high-precision data of *Stracke et al.* [2003] and *Thirlwall et al.* [2004] have been plotted.

sitions. We ascribe the particularly good distribution of our Pb isotopic data among a small number of principal components (see below) to this simple restriction. We note that PCA on Pb isotopes alone is capable of discriminating three components from more than three. If there is an extra, that is a fourth component, it is just a mixture of the other three and contributes to less than 0.05% of the variability in the Pb mixture. In order to minimize the effect of errors and to avoid the uninformative correlations forced by a common small isotope (^{204}Pb), the principal components were calculated using $^{204}Pb/^{206}Pb$, $^{207}Pb/^{206}Pb$, and $^{208}Pb/^{206}Pb$ as raw variables, but we checked that the outcome is not substantially different from that in which the ratios are normalized to ^{204}Pb. The three Pb principal components account for 99, 1, and <0.05%, respectively, of the variance (Figure 10). Including in the analysis the subaerial Iceland samples affects neither the direction of the principal components nor the allocation of the variance among them significantly.

[36] The first Pb principal component is essentially proportional to the $^{206}Pb/^{204}Pb$ ratio (Figures 7 and 11). The second Pb principal component clearly

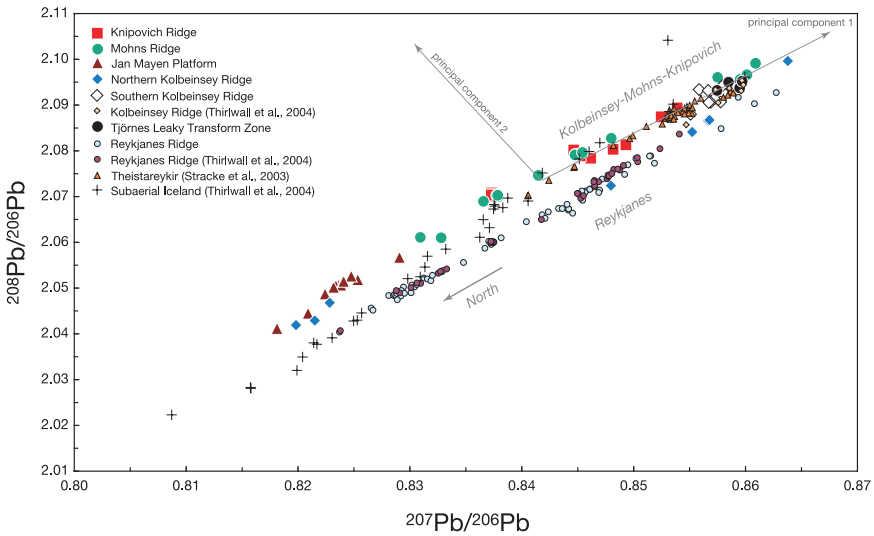

Figure 9. Values of $^{208}Pb/^{206}Pb$ versus $^{207}Pb/^{206}Pb$ for North Atlantic MORB and Iceland. The contrast between MORB north and south of Iceland stands out even more conspicuously than in Figure 8. The two trends link through the most unradiogenic samples from Iceland, the Tjörnes Fracture Zone, and the Kolbeinsey Ridge. The northward trend of decreasing $^{207}Pb/^{206}Pb$ along the Reykjanes Ridge reverts along the Reykjanes Peninsula [*Thirlwall et al.*, 2004] toward the much higher values characteristic of subaerial samples, including Theistareykir [*Stracke et al.*, 2003]. The vectors representing the Pb principal components 1 and 2 have been drawn for reference (see section 6 for details).

separates the ridges north and south of Iceland from each other (Figure 10). The third component is pure noise, which demonstrates that all the data under consideration define a plane in $^{204}Pb/^{206}Pb$-$^{207}Pb/^{206}Pb$-$^{208}Pb/^{206}Pb$ space. To minimize the possible confusion between the standard denomination of the statistical "principal components," which refers to the coordinates of the data along the principal axes of their correlation ellipsoid, and the "geochemical components" of *Zindler and Hart* [1986], we refer in the following to the latter as "end-members." Two significant principal components define a plane and therefore identify a mixing between *three* end-members. When Nd and Hf isotopic data are processed along with the Pb data, a third significant principal component appears and the first three components then account for 82.5, 9.7, and 7.5%, respectively, of the variance. As discussed above, we believe that this *fourth* end-member is an artifact of applying principal component analysis to a non-Euclidian mixing space. Such a smearing of the variability over a larger number of axes contradicts the essentially perfect spread of the Pb isotopic data over a plane in the space of the three Pb isotope plots. It likely reflects both the nonlinear (hyperbolic) mixing relationships when isotopes of different elements are involved and the Nd/Hf/Pb fractionation by fusion and magmatic differentiation. These complex relationships show up in plots such as $^{206}Pb/^{204}Pb$ (a proxy for the first component) versus ε_{Nd} or ε_{Hf} (Figure 12): with the exception of a few of the ridge segments, notably Mohns and Knipovich, these variables form either horizontal or vertical arrays, or just scatter, which is prime evidence that they are uncorrelated.

6.2. Nature of the Pb Principal Components

[37] The vectors corresponding to the first two principal components have been drawn in Figure 13 (and also traced in Figure 9) from the mean value of the Pb isotope compositions of our samples and those of *Thirlwall et al.* [2004] and are shown together with the Pb isotope compositions of our samples singled out. The first component is indistinguishable from the Northern Hemisphere Reference Line of *Hart* [1984] and is therefore essentially controlled by the $^{206}Pb/^{204}Pb$ ratio. This component clearly reflects a mixture of a low-U/Pb depleted mantle end-member (DM) and a second end-member with high time-integrated U/Pb. We therefore also plotted typical basalts from Polynesia considered by *Hofmann* [1997] as type localities for the HIMU end-member together with the C component of *Hanan and Graham* [1996]. As shown by *Hanan and Graham* [1996], the Pb

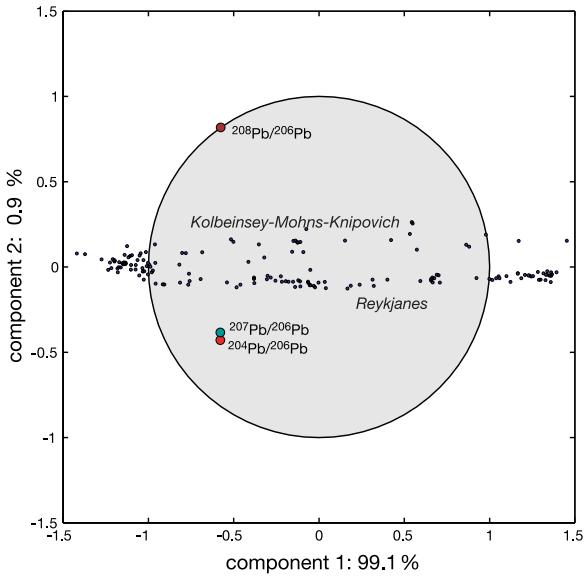

Figure 10. Graphical display of Principal Component Analysis of the Pb isotope data of this study and those of *Thirlwall et al.* [2004]. The first principal component accounts for more than 99% of the total variability of the data set and represents the mixing between DM and C. The second principal component, which represents the addition of EM to the DM-C mixture, accounts for almost all the rest of the variance and clearly separates the ridges north and south of Iceland, as also observed from the raw Pb data in Figures 8 and 9.

isotopic trends of the North Atlantic basalts seem to bundle around a unique point, which led them to postulate the existence of a discrete, but ubiquitous component, which they dubbed "C" for "common" component, in the source of ocean island basalts (OIB). C is in many respects similar to the FOZO component of *Hart et al.* [1992] and the PHEM component of *Farley et al.* [1992], for which the definition also involves He isotope compositions. Our own estimate of C, which was calculated as the intersection between the Arctic and HIMU arrays, falls within errors of the estimate ($^{206}Pb/^{204}Pb$ = 19.8, $^{207}Pb/^{204}Pb$ = 15.60, $^{208}Pb/^{204}Pb$ = 39.45) given by *Hanan and Schilling* [1997]. Figure 13 shows that the HIMU samples plot distinctly *above* the first principal component in the $^{207}Pb/^{204}Pb$ versus $^{206}Pb/^{204}Pb$ diagram, and *below* the first principal component in the $^{208}Pb/^{204}Pb$ versus $^{206}Pb/^{204}Pb$ diagram, whereas the C end-member falls precisely on it. We therefore assume that the first Pb principal component is a mixture between the DM and C end-members. *Hanan and Graham* [1996] argued that mantle containing subducted oceanic crust adequately accounts for the C geochemical end-member.

[38] The second Pb principal component is a subdued "whiff" in Arctic MORB and Iceland basalts (1% of the total variance) and points toward higher $^{208}Pb/^{204}Pb$ ratios (i.e., high Th/U) (Figure 13). Straightforward manipulation of the chronometric equations shows that

$$\frac{d^{208}Pb/^{206}Pb}{d^{207}Pb/^{206}Pb} = \frac{(\lambda_{232Th}/\lambda_{238U})(^{232}Th/^{238}U) - ^{208}Pb/^{206}Pb}{(\lambda_{235U}/\lambda_{238U})(^{235}U/^{238}U) - ^{207}Pb/^{206}Pb},$$

in which the λ's stand for the decay constants of the respective isotopes. This equation demonstrates that the abundance of the second Pb principal component essentially records the Th/U evolution in the mantle source of the basaltic samples. All these characteristics are consistent with the influence of ancient continental detritus. Whether this component betrays subtle contamination by streaks of Archean lithosphere trailing in the upper mantle after the breakup of Pangaea or rather reflects the presence of a genuine recycled component intrinsic to the mantle (Enriched Mantle 2 = EM2) cannot be resolved by the present data.

6.3. Ridge Segmentation

[39] When the Pb principal components are plotted against latitude (Figure 11), the isotopic segmentation of the ridge by Iceland and Jan Mayen into three isotopically identifiable units, (1) the Reykjanes Ridge, (2) the Kolbeinsey Ridge, and (3) the Mohns and Knipovich Ridges, becomes extremely clear. The Hf and Nd isotope data also identify the ridges north and south of Jan Mayen (Figures 5 and 6). The distribution of the Pb principal component 1 on either side of Iceland is strikingly asymmetrical, while it is constant along the Kolbeinsey Ridge, even in the immediate vicinity of Iceland (Figure 11). With the exception of four Reykjanes samples from *Thirlwall et al.* [2004] (Figure 11), the various data sets are remarkably consistent. The Tjörnes Fracture Zone is the southern boundary of the Kolbeinsey MORB mantle and the transition from the Kolbeinsey Ridge to Iceland is marked by an inflexion point of the first Pb principal component. The strong presence of this component in Icelandic basalts seems to be spilling over southward into the Reykjanes Ridge, but not to the north into the Kolbeinsey Ridge.

[40] By contrast, the Pb principal component 2 (EM influence) displays a regular gradient along the Kolbeinsey Ridge (Figure 11) which smoothly merges into *Thirlwall et al.*'s [2004] data on subaerial Iceland. The Kolbeinsey Ridge has a

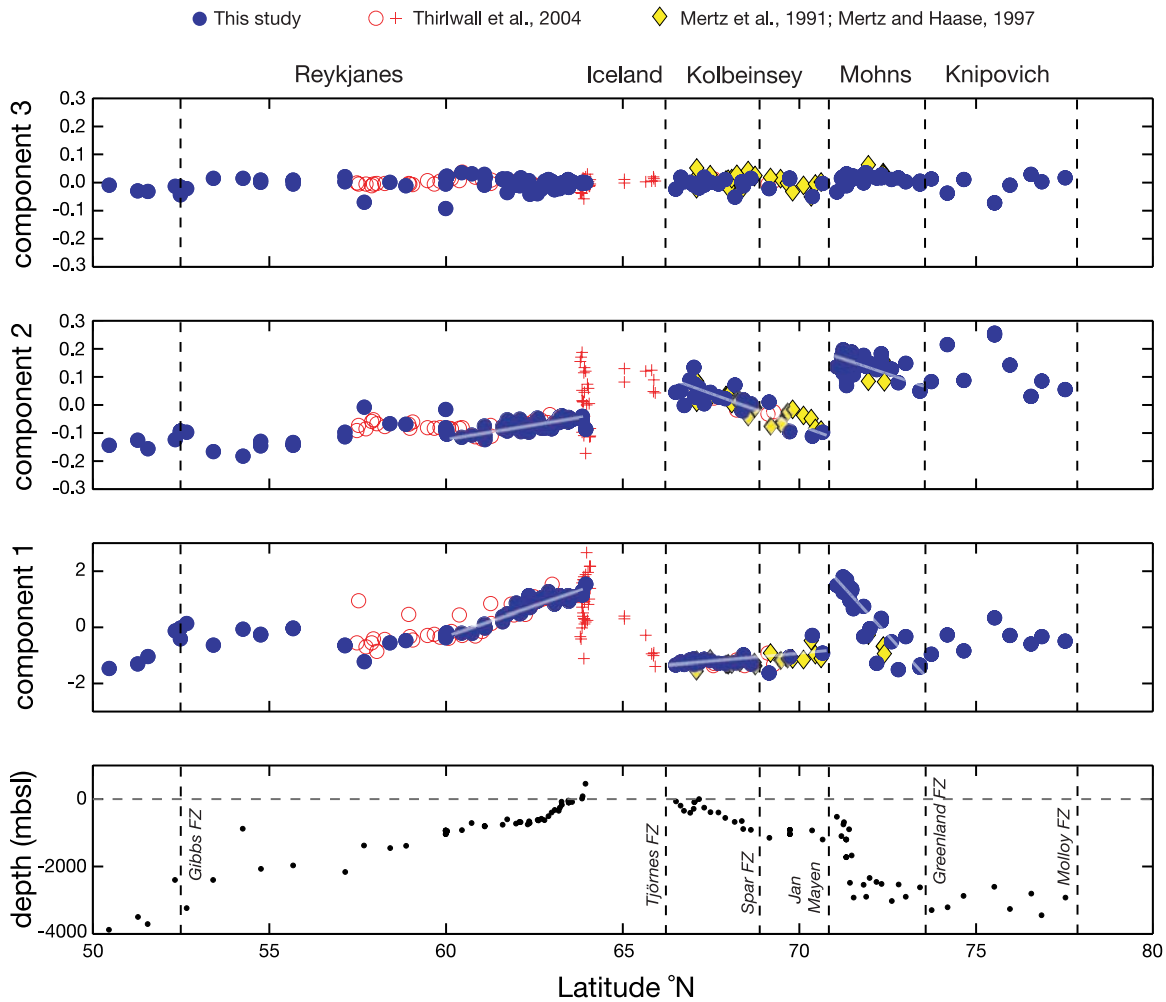

Figure 11. Lead principal components and ridge depth versus latitude. The Pb principal components 1 and 2 are those of Figure 10, while the Pb principal component 3 is pure noise and is not needed for closure of the Pb isotope variability. The lack of a significant third component indicates that the points form an essentially perfect plane in a three-dimensional space of Pb isotopic ratios. Figure 10 is simply a view perpendicular to this plane. Note the factor-of-ten difference in *y* axis scale for the panel of component 1 relative to those of components 2 and 3. The segmentation of the Arctic MAR by Iceland and Jan Mayen into three isotopically distinct units, as indicated by the raw Pb data in Figure 7, stands out quite prominently. The distribution of the Pb principal component 1 on either side of Iceland is strikingly asymmetrical, and its gradient along Kolbeinsey Ridge, even in the immediate vicinity of Iceland, is flat. The values of component 1 along Kolbeinsey grade into those of Iceland with an inflexion point at the Tjörnes Fracture Zone. In contrast, the Pb principal component 2 shows a smooth gradient along the Kolbeinsey Ridge and trends straight into the values for the subaerial Iceland basalts. The break at the Jan Mayen fracture zone affects both of the Pb components and therefore attests to the presence at this locality of a major mantle discontinuity. Component 1 spreads southward from Iceland into the Reykjanes Ridge and northward from Jan Mayen into the Mohns Ridge. The two Pb components therefore seem to be associated with distinct geodynamic carriers. The straight line segments with light-colored shade going through the data points highlight geochemically coherent ridge segments.

higher $^{208}Pb/^{206}Pb$ for a given $^{207}Pb/^{206}Pb$ than the Reykjanes Ridge [*Mertz et al.*, 1991], or, equivalently, contains more of the Pb principal component 2. A similar argument can be made using the $^{208}Pb/^{204}Pb$-$^{207}Pb/^{204}Pb$ contrast identified between Iceland and Kolbeinsey by *Thirlwall* [1995]. The second Pb principal component, also clearly visible in Icelandic basalts, appears to spread northward into the Kolbeinsey Ridge, but does not seem to affect the Reykjanes Ridge. The Icelandic plume thus seems to sort out components in different systems in different directions: the halo

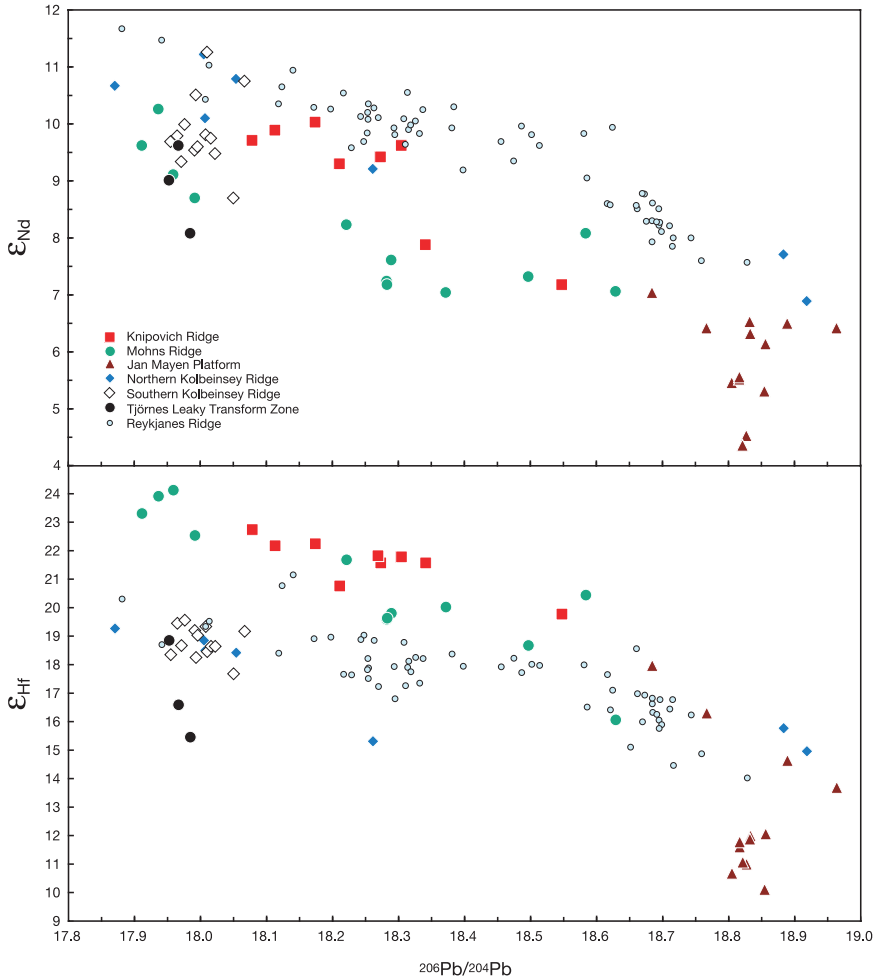

Figure 12. Values of ε_{Nd} and ε_{Hf} versus $^{206}Pb/^{204}Pb$ for North Atlantic MORB of this study. Except for the Mohns and Knipovich Ridges, and only to some extent, the other ridge segments display either near-horizontal or -vertical arrays, or just scatter, which is evidence for overall lack of first-order correlation between Hf and Nd isotopes on the one hand and Pb isotopes on the other hand.

polluted by Hf and Nd (and Sr and He) of presumably Icelandic origin extends over ~1 degree along the Kolbeinsey Ridge in contrast to ~5 degrees along the Reykjanes Ridge. Different geochemical end-members present in the Icelandic plume therefore appear to be entrained into the northern and southern ridges in opposite directions. The striking decoupling between the Pb components on the one hand and Hf and Nd (and Sr and He) isotopes on the other hand may be revealing a so-far unsuspected structure (zoning) within the Iceland plume.

[41] The Pb, Nd, and Hf isotopic ratios of MORB from the Reykjanes ridge at ~55°N are similar to those of the Kolbeinsey Ridge, thus defining the isotopic "base level" for the local asthenosphere when unaffected by plumes. However, although the Iceland hot spot affects the isotope geochemistry of its neighboring ridges in a very distinct way, there is no strong evidence for a geochemical discontinuity in the underlying mantle. By contrast, the Jan Mayen Fracture Zone clearly seems to be a major geochemical mantle boundary for both of the Pb components (Figure 11) and also for Nd and Hf (Figure 5). Even if transitional samples have been described [*Schilling et al.*, 1999], the overall distribution of the Pb components on either side of Jan Mayen highlights the presence of a geochemical discontinuity coinciding with a dramatic break in bathymetry (Figure 11, lowermost panel). This boundary is likely to separate upwelling asthenospheric masses with very different histories in much the same way as the Australian-Antarctic

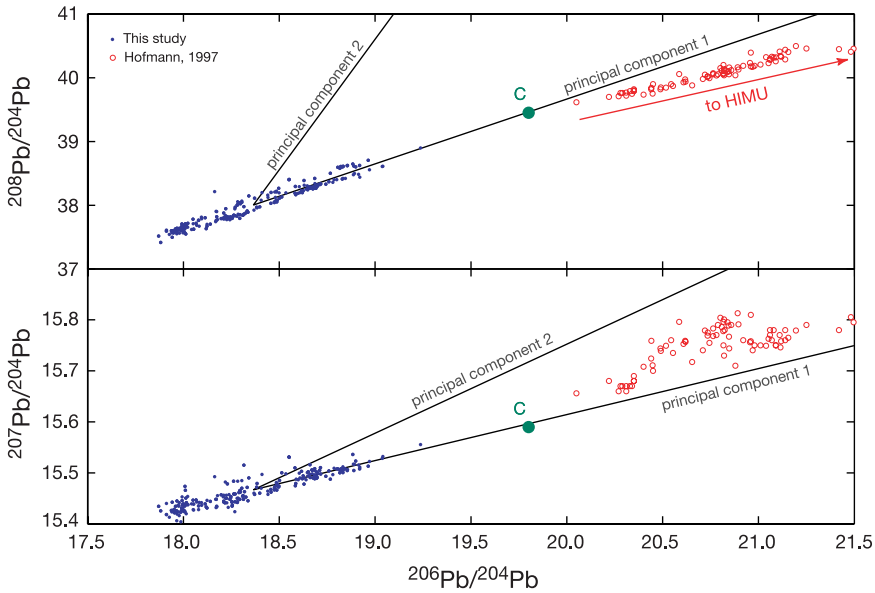

Figure 13. Projection of the first two principal component vectors drawn from the mean value of Pb isotope compositions of North Atlantic MORB (this study and *Thirlwall et al.* [2004]) shown together with the Pb isotope compositions of the samples of this study. The first component is indistinguishable from the Northern Hemisphere Reference Line of *Hart* [1984] and reflects a mixture between a low-U/Pb depleted mantle end-member (DM) and a second end-member (EM) with high time-integrated U/Pb. *Hanan and Graham*'s [1996] C component is clearly a better representative of the high-U/Pb end-member than the HIMU (high-U/Pb) basalts compiled by *Hofmann* [1997].

Discordance separates Indian from Pacific mantle [*Klein et al.*, 1988] and the Easter Microplate separates two distinct types of Pacific mantle [*Vlastélic et al.*, 1999].

6.4. Mixing North of Jan Mayen

[42] Mixing relationships along the Mohns Ridge reinforce *Hanan and Graham*'s [1996] arguments for the existence of the C end-member. Demonstrating that an intermediate convergence point such as "C" owes its existence to a physically identifiable component, or end-member, rather than the necessary focusing around an elusive mean value, is a difficult challenge. A straightforward interpretation is that the curved trend in ε_{Hf}-ε_{Nd} space defined by MORB dredged along the Mohns Ridge, and possibly also MORB dredged along the Knipovich Ridge, and the Jan Mayen Platform (Figure 6) may reflect a nearly binary mixing with the least unradiogenic component lying within the mantle array. Figure 6 shows the mixing hyperbola in an $x = \varepsilon_{Nd}$, $y = \varepsilon_{Hf}$ plot with the equation

$$(\varepsilon_{Hf} - y_\infty)(\varepsilon_{Nd} - x_\infty) = c.$$

Using a least squares fit through the ε_{Hf}-ε_{Nd} data, we found that the asymptotes of this hyperbola are positioned at $y_\infty = 30.1 \pm 0.9$ and $x_\infty = 4.2 \pm 0.8$ and that its curvature factor $c = -34 \pm 6$ [*Albarède*, 1995]. Because of the strong curvature of the hyperbola, the Nd isotope composition of the least radiogenic end-member is rather well defined (~+6, point A in Figure 6). If this component is common to the Reykjanes-Iceland-Kolbeinsey trend and this mixing hyperbola, then its ε_{Hf} value must be ~+11. Such an end-member clearly belongs in the OIB clan and, despite $^3He/^4He$ values of ~+7 to +8, is distinctly uncharacteristic of a MORB source. The ε_{Nd} and ε_{Hf} coordinates of point A (+6 and +11, respectively) fall well within the average mantle array. Furthermore, the values for point A are indistinguishable from those (ε_{Hf} = +10 and ε_{Nd} = +5) assigned to the C component [*Hanan et al.*, 2000; *Andres et al.*, 2002], which supports the contention that C (and thus FOZO and PHEM) is a real internal mantle component.

[43] The second end-member of the mixing hyperbola is highly depleted and its ε_{Hf}-ε_{Nd} isotope composition (point B in Figure 6) must be assumed. The quotient of the Hf/Nd ratios between the two end-members A and B can be calculated using, for example, the equations of section 1.3.3 of *Albarède* [1995]:

$$\frac{(Hf/Nd)_B}{(Hf/Nd)_A} = \frac{(x_\infty y_\infty - x_B y_A - c)}{(x_\infty y_\infty - x_A y_B - c)}.$$

For an ε_{Nd} value of ~+10.5 (and therefore ε_{Hf} of +24.7), we find that the Hf/Nd ratio of the

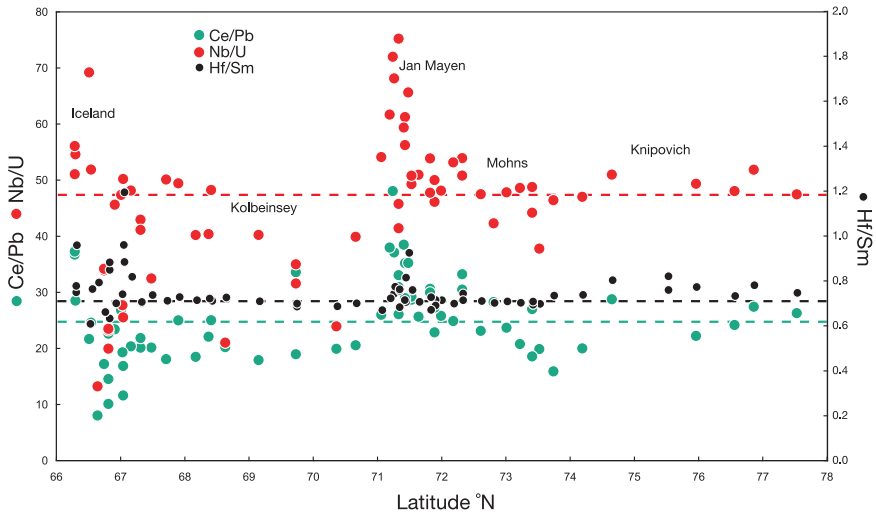

Figure 14. Values of Ce/Pb, Nb/U, and Hf/Sm versus latitude for MORB north of Iceland. Ce/Pb and Nb/U north of Jan Mayen are overall similar to mantle values (green and red stippled lines). Likewise, the Hf/Sm ratio, which is a particularly sensitive indicator of the involvement of zircon-depleted or -enriched sediment, is around the planetary value of 0.72 (black stippled line) for all samples. Trace element data are from this study, *Schilling et al.* [1999], *Hanan et al.* [2000], and URI, unpublished data.

radiogenic end-member is 3.5 times that of the unradiogenic end-member, which we have tentatively identified with C. The exact value assumed for ε_{Nd} of the radiogenic end-member does not greatly affect this result since the quotient increases to only 4.3 for ε_{Nd} of +12. Moreover, as will be seen below, the important observation is not the actual value of the Hf/Nd quotient, but that the Hf/Nd ratio of the radiogenic end-member is *higher*, not *lower*, than that of the unradiogenic end-member.

[44] Because the Mohns and Knipovich Ridges are located not far from the Baltic and Svalbard-Barents Sea continental shelf breaks, the nature of this radiogenic end-member raises the issue of the presence in the MORB source of continental crust. Seismological data have been interpreted as signaling crustal remnants beneath the Jan Mayen plateau [*Kodaira et al.*, 1998]. However, as originally argued by *Trønnes et al.* [1999], using trace elements, there is no strong indication that the present MORB samples are pervasively polluted by a component resembling true continental crust. The low $^{206}Pb/^{204}Pb$ ratio (<18.0) of the B end-member (Figure 12) fits only with the granulitic section of continental crust. In addition, along and north of the Jan Mayen Platform, the Ce/Pb and Nb/U ratios [*Schilling et al.*, 1999; *Hanan et al.*, 2000; URI, unpublished data] show values similar to those (25 and 48, respectively) of the canonical mantle values of *Hofmann et al.* [1986] (Figure 14). Even the $^{3}He/^{4}He$ signal, which reaches an overall low in the vicinity of Jan Mayen at about 6.8–8.1 times the atmospheric ratio [*Schilling et al.*, 1999], is still very MORB-like.

[45] An alternative possibility is that the assumed crustal component is an integral part of the mantle source of basalts. Radiogenic Hf combined with relatively unradiogenic, that is normal Nd (as in end-member B) is the hallmark of pelagic sediment involvement [*Patchett et al.*, 1984; *Albarède et al.*, 1998]. Because deep-sea clays are deficient in zircon with respect to regular continental crust, Hf/Sm ratios can be used to fingerprint a contribution from pelagic material [*White and Duncan*, 1996]. The Hf/Sm ratios of MORB north of Jan Mayen [*Schilling et al.*, 1999; this study, Table 1] cluster around the canonical planetary value of 0.72 [*Blichert-Toft et al.*, 2002] (Figure 14). This, combined with the evidence from Figure 6 that the Hf/Nd ratio in the radiogenic end-member (B) is ~3.5 times *higher* than that of the unradiogenic end-member (A), corroborates the conclusion that pelagic sediments do not contribute visibly to the source of the local MORB.

[46] The unusually radiogenic Hf isotope compositions of Mohns and Knipovich MORB and the remarkable scatter of the data along these two ridge segments therefore make them unique and, in particular, distinct from the components involved

on both sides of Iceland. Despite their strong source depletion, as attested to by the Nd and especially the Hf isotope ratios, the apparent LREE enrichment of the Mohns and Knipovich MORB requires smaller-degree melts with respect to Kolbeinsey MORB [*Haase et al.*, 1996; *Schilling et al.*, 1999]. Small-degree melts and shallow asthenospheric upwelling associated with a slow spreading rate [*Gripp and Gordon*, 2002] result from a combination of the strongly oblique spreading of the Mohns Ridge [*Géli et al.*, 1994] and a rather high latitude with respect to the Eulerian pole of the Europe-North America opening (62′4°N 135′8°E) [*Gordon*, 1995]. As discussed previously by a number of authors [e.g., *Salters and Hart*, 1989; *Salters and Zindler*, 1995; *Blichert-Toft and Albarède*, 1997; *Chauvel and Blichert-Toft*, 2001], Hf-Nd isotope decoupling is readily accomplished by garnet fractionation. If melting takes place at equilibrium, the isotopic composition is dictated by the whole rock. The presence of garnet in the residual assemblage is therefore irrelevant and the source itself must be anomalous. Unusually radiogenic Hf at a specific value of $^{143}Nd/^{144}Nd$ may signal the presence in the source of ancient LREE-depleted cumulates, such as garnet pyroxenite or garnet peridotite. Such residues from ancient melt extraction events at great depth, where garnet/clinopyroxene ratios would have been high, would be likely to have not only the high Hf/Nd ratios observed for the Mohns-Knipovich Ridge basalts, but also the high Lu/Hf and higher-than-usual (Lu/Hf)/(Sm/Nd) required for these samples to have grown in their highly radiogenic Hf and produced the distinctive Hf-Nd isotope decoupling we observe. Melting of garnet-rich cumulates is unfortunately not consistent with the unradiogenic character of Pb in the radiogenic-Hf component. *Beattie* [1993] and *Hauri et al.* [1994] found that upon crystal/liquid fractionation, Pb is much more depleted in garnet than U and these cumulates should quickly evolve fairly high $^{206}Pb/^{204}Pb$ ratios, which is not the case. An alternative possibility that could account for a component with radiogenic Hf and Nd and the high Hf/Nd ratio visible in the Mohns-Knipovich Ridge basalts would be a source of strongly residual character, but since the Nd in these samples is not particularly radiogenic with respect to most other MORB, such a scenario is less likely.

[47] A disturbing aspect of the high-ε_{Hf} samples north of Jan Mayen is that they hint at an additional depleted end-member (point B in Figure 6) apparently absent from the Pb principal components. We therefore examine the alternative possibility that point B is not a real end-member, implying that the hyperbola between points A and B does not necessarily reflect a truly binary mixing relationship (which would account for the lack of strong variation in Hf/Nd along these ridge segments). In such a scenario, disequilibrium melting is responsible for the very particular scatter of Hf isotopes in the most depleted rocks. The merits of disequilibrium melting were recently reinvestigated by *van Orman et al.* [2001], who suggested that Nd isotope equilibration takes up to 1 Gyr at the eclogite solidus (1150°C). If the parameters for Th^{4+} diffusion [*van Orman et al.*, 1998] can be used as proxies for Hf, Hf^{4+} can be expected to show even greater disequilibrium effects. Divalent (Pb^{2+}) and trivalent (Nd^{3+}) elements are probably less prone to kinetic effects. Disequilibrium melting is advantageous in that it relieves the requirement of a distinct geochemical end-member in the MORB source. Hafnium in garnet from peridotite inclusions in kimberlites can be extremely radiogenic, with $\varepsilon_{Hf}(0)$ of up to +1000, such as observed in Canadian and South African samples [*Schmidberger et al.*, 2002; *Bedini et al.*, 2004]. Neodymium from the same samples is radiogenic as well, but to a far lesser extent, which suggests that the closure temperature in garnet is higher for the Lu-Hf than the Sm-Nd system. In addition, observations on peridotites show that interaction with small melt fractions fails to equilibrate Hf and Nd isotopes among the minerals of peridotites [*Simon et al.*, 2003; *Bedini et al.*, 2004; *Frey et al.*, 2004]. Any isotopic disequilibrium during garnet breakdown, in particular during incongruent melting across the garnet-spinel transition, such as $\text{Garnet} + \text{Liquid}_1 \iff \text{Spinel} + \text{Liquid}_2$, would therefore tend to produce melts with Hf isotope compositions particularly radiogenic with respect to those of the accompanying Nd. Radiogenic Hf released by garnet breakdown is expected to migrate upward more efficiently than less abundant radiogenic Nd or common Hf locked up in clinopyroxene. This interpretation also holds, although to a smaller extent, for clinopyroxene, since in spinel peridotite inclusions from Hawaiian alkali basalts, clinopyroxene is known to contain Hf substantially more radiogenic than predicted from its corresponding Nd isotope compositions [*Salters and Zindler*, 1995].

[48] The unusual character of this high-ε_{Hf} end-member suggests an unusual source. From the high levels of labile elements in basalts from the Mohns Ridge, *Haase et al.* [1996] argued that the nearby

subcontinental Greenland lithosphere contributed to their genesis. A contribution of low-degree melts from trailing streaks of old Greenlandic or European subcontinental lithospheric mantle caught in the upwelling asthenosphere beneath the Mohns and Knipovich Ridges combined with some measure of disequilibrium during melting is a possibility. In their Atlantic-wide study of isotopic gradients, *Andres et al.* [2004], though without invoking disequilibrium melting as the source of isotopic decoupling, also attributed the long-wavelength Hf-Nd trend in MORB to a gradient in the amount of subcontinental mantle material affecting their source. Because the Mohns and Knipovich Ridges are extremely close to the continents, it makes intuitive sense that they should also have the strongest signal of this ancient subcontinental mantle, which is tapped most readily where the continents are rifting apart.

6.5. Is Jan Mayen a Hot Spot?

[49] If the Jan Mayen Platform contains no appreciable contribution from continental crust, what then is its actual nature? The distribution of Nd and Hf isotope compositions (Figure 5) and the first Pb principal component (Figure 11) on both sides of the Jan Mayen fracture zone is consistent with a model in which hot spot material is injected and expands into the Mohns Ridge. The strong discontinuity observed for the second Pb principal component (Figure 11), however, indicates that this material is injected along a major mantle boundary. As for Iceland, the two Pb components seem to have distinct mantle dynamics. Whether the Jan Mayen Island and its southern extension, the Jan Mayen Ridge, represent the trace of a hot spot is strongly disagreed upon in the literature. It has been known for a couple of decades [*Bott*, 1985] that some 25 Myr ago, the MAR north of Iceland jumped from its original position on the now fossil Aegir Ridge to its current position on the Kolbeinsey Ridge. The broad stretch of crust left behind in between these two ridges, known as the Icelandic Plateau, is now crowned by the Jan Mayen Ridge. In Figure 1, we have plotted the trace of the European lithospheric movement over the hot spot reference frame during the last 25 Myr using the poles and velocities of *Gripp and Gordon* [2002]. Although the estimated vector representing this displacement is affected by substantial uncertainty, it is clearly distinct from the direction of the Jan Mayen Ridge. If this ridge is not a hot spot track, it could be the remnant of an early Icelandic oceanic plateau formed in the aftermath of the continental breakup, first separated from the Faeroe-Vøring Bank by the rifting of the Aegir Ridge, then from the East Greenland volcanic province by the rifting of the Kolbeinsey Ridge. This interpretation would account for the unusual seismic structure of the Jan Mayen Ridge [*Kodaira et al.*, 1998] and for the lack of a continental signature in the basalts around Jan Mayen, but hardly explains why the Jan Mayen Island is still volcanically active.

7. Conclusions

[50] On the basis of principal component analysis, precisely three geochemical end-members account for >99.95% of the Pb isotope variability in Arctic and Icelandic basalts. Some decoupling of Pb from Hf and Nd isotopes is apparent, which is due partly to the nonlinear mixing relationship between isotopic compositions of different elements and partly to elemental fractionation during melting. The first Pb principal component reflects a mixture of two geochemical end-members, the depleted mantle (asthenosphere or DM) and "C" [*Hanan and Graham*, 1996]. The second Pb principal component reflects the presence of a third enriched end-member (EM) with a distinct Th/U ratio.

[51] The MAR appears to be divided into three isotopically distinct segments separated by Iceland and Jan Mayen. The strong first Pb principal component present in Icelandic basalts seems to be spilling over southward into the Reykjanes Ridge, but not to the north into the Kolbeinsey Ridge. Hf and Nd isotopes mirror the first Pb principal component. By contrast, the gradient between subaerial Iceland and Kolbeinsey basalts is fairly smooth for the second Pb principal component. As for Iceland, the two components present in basalts around Jan Mayen seem to have different dynamics, with the first Pb principal component and its Nd and Hf counterparts spreading exclusively northward into the Mohns Ridge.

[52] Basalts north of Jan Mayen display the most consistently radiogenic Hf reported up to now for any MORB worldwide. The curved Hf-Nd isotope array along the Mohns Ridge represents mixing between C and a high-ε_{Hf} end-member, which could be basalts produced by disequilibrium melting of garnet- or clinopyroxene-bearing peridotites. One option is that streaks of subcontinental lithosphere left by continental rifting are present in the North Atlantic mantle.

[53] Trace element data argue against the presence of substantial masses of continental crust beneath Jan Mayen. The new isotopic data presented here also provide no evidence against the hypothesis that Jan Mayen is a hot spot. If this is indeed the case, material is injected along a major mantle discontinuity.

Appendix A: Summary of Previous Work on the Arctic MAR

[54] The progressive northward decrease to very low values of spreading rate, ridge axis elevation, and mean degree of melting along the Arctic MAR has been noticed to take place in a stepwise fashion over the Kolbeinsey, Mohns, and Knipovich Ridges [*Schilling et al.*, 1999]. The isotopic and geochemical nature of the underlying mantle, as revealed by the detailed sampling along these ridge segments, was observed to be highly diverse and of distinctive length scales [*Schilling et al.*, 1983; *Neumann and Schilling*, 1984; *Waggoner*, 1990; *Mertz et al.*, 1991; *Devey et al.*, 1994; *Haase et al.*, 1996; *Mertz and Haase*, 1997; *Schilling et al.*, 1999; *Trønnes et al.*, 1999]. The possible reasons for the extremely heterogeneous nature of the mantle in the Arctic Atlantic region have been disputed at length.

[55] While *Schilling et al.* [1999] most recently suggested that chemical and isotopic variations along the Kolbeinsey and Mohns Ridges could be attributed to the distinct influence of, respectively, the Iceland and the Jan Mayen mantle plumes, others [*Mertz et al.*, 1991; *Haase et al.*, 1996] held that the observed variations more likely were due to a heterogeneous MORB mantle source consisting of enriched and depleted components with distinct melting characteristics, combined with cold edge effects from fracture zones or continental fragments. Yet others [*Haase et al.*, 1996; *Trønnes et al.*, 1999] did not acknowledge the existence of the Jan Mayen plume, but proposed a hybrid model in which large-scale dispersion of the Iceland mantle plume alone accounts for the observed variability. Finally, involvement of randomly distributed continental lithosphere material entrained in the melting regime beneath the immature Knipovich Ridge, due to its proximity to the Barents Sea-Svalbard continental platform, has been considered to explain the large and scattered chemical and isotopic variations along this ridge segment [*Schilling et al.*, 1999]. On the basis of the available geochemical data (major and trace elements and Sr, Nd, conventional Pb, and He isotope compositions) of this series of studies, it was not possible to discriminate between these different, all plausible scenarios.

[56] The apparent lack of a Pb isotope gradient along the Kolbeinsey Ridge from 67°N to 69°N, which stood in stark contrast to gradually varying Sr and Nd isotope ratios, further prompted *Mertz et al.* [1991] to suggest that the Tjörnes Transform Zone is blocking any northward flow and mixing of the Iceland plume with the depleted upper mantle beneath the Kolbeinsey Ridge, thus suggesting an asymmetric plume dispersion along the MAR, as also apparently indicated by previously reported REE data [*Schilling et al.*, 1983]. Instead, the companion gradients in Sr and Nd isotope and U/Pb ratios observed between the Spar and Tjörnes Transform Zones led Mertz and coauthors to suggest a southward flow toward Iceland composed of an unusual two-component MORB mantle source type. Trace element data on this same sample suite were later used to model the variations by dynamical, fractional decompression melting of a lherzolitic upper mantle, with successive pooling of melts at different depths within the garnet and spinel lherzolite facies from 80 to 30 km [*Devey et al.*, 1994].

[57] *Haase et al.* [1996] subsequently applied trace element data from independently collected alkali basalts from the Jan Mayen Platform and tholeiites from the Mohns Ridge around 72°N to argue against the presence of a Jan Mayen hot spot mantle plume. Instead, these authors evoked production of small-degree melts from a metasomatized mantle source, supposedly heterogeneous on a small scale, caused by cold edge effects due to the combined presence of the Jan Mayen Fracture Zone and a continental fragment, presumably present beneath the paleo-Jan Mayen Ridge.

[58] Contrary to the original study by *Mertz et al.* [1991], the following more extensive Sr-Nd-Pb-He isotope study by *Schilling et al.* [1999], which in addition included basalts from the Tjörnes Transform Zone, revealed a steep Pb isotope gradient increasing toward Iceland across the Tjörnes Transform Zone, thus apparently ruling out any significant dampening effect northward of the dispersing Iceland mantle plume by this transform fault. These results were interpreted to reflect a northward flow with melting and mixing of the Iceland mantle plume with the depleted upper mantle, extending up to the Spar Fracture Zone. The 200 km longer (with respect to the Sr-Nd-Pb gradients) $^{3}He/^{4}He$ gradient further led these authors to suggest that the ''nose'' of the mantle plume may actually extend

beyond the Spar Fracture Zone, without melting taking place, but partly degassing at greater depth. The two nearly mirror-image gradients in Sr-Nd-Pb isotope space observed along the northern Kolbeinsey and Mohns Ridges, on each side of the Jan Mayen Platform, were proposed to reflect not only the influence of the Jan Mayen plume, but also its radial dispersion and mixing with the surrounding depleted upper mantle.

[59] Rather than calling upon the influence of the two separate mantle plumes of Iceland and Jan Mayen to interpret the along-MAR isotopic variations, *Trønnes et al.* [1999], in their simultaneous study of Jan Mayen basalts, suggested that the observed isotopic variability be caused by a very broad dispersion of the Iceland mantle plume reaching as far as, and perhaps beyond, Jan Mayen, and the added effects of lithosphere variations on the extent of partial melting. They proposed that, beneath the Jan Mayen Platform, the rising mantle column is truncated at a depth of ~90 km, resulting in the final separation of very small-degree melts of the most fusible component of the Iceland plume, whereas along the surrounding MAR, greater decompression melting and dilution by melting of the peridotite matrix occurs.

Acknowledgments

[60] We thank Urszula Tomza for assistance in the chemistry lab at URI and Philippe Télouk for help with the Plasma 54 at ENSL. We are grateful for constructive reviews by Barry Hanan and Vincent Salters and for useful criticism and suggestions from the two editors, Bill White and Dave Graham. We acknowledge financial support from the French Institut National des Sciences de l'Univers and the US National Science Foundation.

References

Abouchami, W., S. J. G. Galer, and A. W. Hofmann (2000), High precision lead isotope systematics of lavas from the Hawaiian Scientific Drilling Project, *Chem. Geol.*, *169*, 187–209.

Albarède, F. (1995), *Introduction to Geochemical Modeling*, 543 pp., Cambridge Univ. Press, New York.

Albarède, F., A. Simonetti, J. D. Vervoort, J. Blichert-Toft, and W. Abouchami (1998), A Hf-Nd isotopic correlation in ferromanganese nodules, *Geophys. Res. Lett.*, *25*, 3895–3898.

Albarède, F., P. Télouk, J. Blichert-Toft, M. Boyet, A. Agranier, and B. Nelson (2004), Precise and accurate isotopic measurements using multiple-collector ICPMS, *Geochim. Cosmochim. Acta*, *68*, 2725–2744.

Albarède, F., A. Stracke, V. J. M. Salters, D. Weis, J. Blichert-Toft, P. Télouk, and A. Agranier (2005), Comment to "Pb isotopic analysis of standards and samples using a ^{207}Pb-^{204}Pb double spike and thallium to corrrect for mass bias with a double-focusing MC-ICP-MS" by Baker et al., *Chem. Geol.*, in press.

Andres, M., J. Blichert-Toft, and J. Schilling (2002), Hafnium isotopes in basalts from the southern Mid-Atlantic Ridge from 40°S to 55°S: Discovery and Shona plume-ridge interactions and the role of recycled sediments, *Geochem. Geophys. Geosyst.*, *3*(10), 8502, doi:10.1029/2002GC000324.

Andres, M., J. Blichert-Toft, and J.-G. Schilling (2004), Nature of the depleted upper mantle beneath the Atlantic: Evidence from Hf isotopes in normal mid-ocean ridge basalts from 79°N to 55°S, *Earth Planet. Sci. Lett.*, *225*, 89–103.

Baker, J., D. Peate, T. Waight, and C. Meyzen (2004), Pb isotopic analysis of standards and samples using a ^{207}Pb-^{204}Pb double spike and thallium to correct for mass bias with a double-focusing MC-ICP-MS, *Chem. Geol.*, *211*, 275–303.

Beattie, P. (1993), Uranium-thorium disequilibria and partitioning on melting of garnet peridotite, *Nature*, *363*, 63–65.

Bedini, R.-M., J. Blichert-Toft, M. Boyet, and F. Albarède (2004), Isotopic constraints on the cooling of the continental lithosphere, *Earth Planet. Sci. Lett.*, *223*, 99–111.

Blichert-Toft, J., and F. Albarède (1997), The Lu-Hf isotope geochemistry of chondrites and the evolution of the mantle-crust system, *Earth Planet. Sci. Lett.*, *148*, 243–258.

Blichert-Toft, J., C. Chauvel, and F. Albarède (1997), Separation of Hf and Lu for high-precision isotope analysis of rock samples by magnetic sector-multiple collector ICP-MS, *Contrib. Mineral. Petrol.*, *127*, 248–260.

Blichert-Toft, J., M. Boyet, P. Télouk, and F. Albarède (2002), ^{147}Sm-^{143}Nd and ^{176}Lu-^{176}Hf in eucrites and the differentiation of the HED parent body, *Earth Planet. Sci. Lett.*, *204*, 167–181.

Blichert-Toft, J., D. Weis, C. Maerschalk, A. Agranier, and F. Albarède (2003), Hawaiian hot spot dynamics as inferred from the Hf and Pb isotope evolution of Mauna Kea volcano, *Geochem. Geophys. Geosyst.*, *4*(2), 8704, doi:10.1029/2002GC000340.

Bott, M. H. P. (1985), Plate tectonic evolution of the Icelandic transverse ridge and adjacent regions, *J. Geophys. Res.*, *90*, 9953–9960.

Castillo, P. (1988), The Dupal anomaly as a trace of the upwelling lower mantle, *Nature*, *336*, 667–670.

Chauvel, C., and J. Blichert-Toft (2001), A hafnium isotope and trace element perspective on melting of the depleted mantle, *Earth Planet. Sci. Lett.*, *190*, 137–151.

Chauvel, C., and C. Hémond (2000), Melting of a complete section of recycled oceanic crust: Trace element and Pb isotopic evidence from Iceland, *Geochem. Geophys. Geosyst.*, *1*, doi:10.1029/1999GC000002.

Christensen, U. R., and A. W. Hofmann (1994), Segregation of subducted oceanic crust in the convecting mantle, *J. Geophys. Res.*, *99*, 19,867–19,884.

Davies, G. F. (2002), Stirring geochemistry in mantle convection models with stiff plates and slabs, *Geochim. Cosmochim. Acta*, *66*, 3125–3142.

Devey, C. W., C.-D. Garbe-Schönberg, P. Stoffers, C. Chauvel, and D. F. Mertz (1994), Geochemical effects of dynamic melting beneath ridges: Reconciling major and trace element variations in Kolbeinsey (and global) mid-ocean ridge basalt, *J. Geophys. Res.*, *99*, 9077–9095.

Dupré, B., and C. J. Allègre (1983), Pb-Sr isotope variation in Indian Ocean basalts and mixing phenomena, *Nature*, *303*, 142–146.

Eisele, J., W. Abouchami, S. J. G. Galer, and A. W. Hofmann (2003), The 320 kyr Pb isotope evolution of Mauna Kea lavas recorded in the HSDP-2 drill core, *Geochem. Geophys. Geosyst.*, *4*(5), 8710, doi:10.1029/2002GC000339.

Eldholm, O., J. Thiede, and E. Taylor (1989), Evolution of the Vøring volcanic margin, *Proc. Ocean. Drill. Program Sci. Results*, *104*, 1033–1065.

Farley, K. A., J. H. Natland, and H. Craig (1992), Binary mixing of enriched and undegassed (primitive?) mantle components (He, Sr, Nd, Pb) in Samoan lavas, *Earth Planet. Sci. Lett.*, *111*, 183–199.

Ferrachat, S., and Y. Ricard (1998), Regular vs. chaotic mantle mixing, *Earth Planet. Sci. Lett.*, *155*, 75–86.

Frey, F. A., S. Huang, J. Blichert-Toft, M. Regelous, and M. Boyet (2004), Origin of depleted components in basalt related to the Hawaiian hotspot: Evidence from isotopic and incompatible element ratios, *Geochem. Geophys. Geosyst*, doi:10.1029/2004GC000757, in press.

Géli, L., V. Renard, and C. Rommevaux (1994), Ocean crust formation processes at very slow spreading centers: A model for the Mohns Ridge, near 72°N, based on magnetic, gravity, and seismic data, *J. Geophys. Res.*, *99*, 2995–3013.

Gordon, R. G. (1995), Present plate motions and plate boundaries, in *Global Earth Physics: A Handbook of Physical Constants*, vol. 1, edited by T. J. Ahrens, pp. 66–87, AGU, Washington, D. C.

Govindaraju, K. (1994), Compilation of working values and sample description for 383 geostandards, *Geostand. Newsl.*, *18*, 1–158.

Gripp, A. E., and R. G. Gordon (2002), Young tracks of hotspots and current plate velocities, *Geophys. J. Int.*, *150*, 321–361.

Gurnis, M., and G. F. Davies (1986), The effect of depth-dependent viscosity on convective mixing in the mantle and the possible survival of primitive mantle, *Geophys. Res. Lett.*, *13*, 541–544.

Haase, K. M., C. W. Devey, D. F. Mertz, P. Stoffers, and D. Garbe-Schönberg (1996), Geochemistry of lavas from Mohns Ridge, Norwegian-Greenland Sea: Implications for melting conditions and magma sources near Jan Mayen, *Contrib. Mineral. Petrol.*, *123*, 223–237.

Hanan, B. B., and D. W. Graham (1996), Lead and helium isotope evidence from oceanic basalts for a common deep source of mantle plumes, *Science*, *272*, 991–995.

Hanan, B. B., and J.-G. Schilling (1997), The dynamic evolution of the Iceland mantle plume: The lead isotope perspective, *Earth Planet. Sci. Lett.*, *151*, 43–60.

Hanan, B. B., J. Blichert-Toft, R. Kingsley, and J. Schilling (2000), Depleted Iceland mantle plume geochemical signature: Artifact of multicomponent mixing?, *Geochem. Geophys. Geosyst.*, *1*, doi:10.1029/1999GC000009.

Hanan, B. B., J. Blichert-Toft, D. G. Pyle, and D. M. Christie (2004), Contrasting origins of the upper mantle revealed by hafnium and lead isotopes from the Southeast Indian Ridge, *Nature*, *432*, 91–94. (Corrigendum, *Nature*, *432*, 653, 2004.)

Hart, S. R. (1984), A large-scale isotope anomaly in the southern hemisphere mantle, *Nature*, *309*, 753–757.

Hart, S. R., E. H. Hauri, L. A. Oschmann, and J. A. Whitehead (1992), Mantle plumes and entrainment: Isotopic evidence, *Science*, *256*, 517–520.

Hauri, E. H., T. P. Wagner, and T. L. Grove (1994), Experimental and natural partitioning of Th, U, Pb and other trace elements between garnet, clinopyroxene and basaltic melts, *Chem. Geol.*, *117*, 149–166.

Hofmann, A. W. (1997), Mantle geochemistry: The message from oceanic volcanism, *Nature*, *385*, 219–229.

Hofmann, A. W., K. P. Jochum, M. Seufert, and W. M. White (1986), Nb and Pb in oceanic basalts: New constraints on mantle evolution, *Earth Planet. Sci. Lett.*, *79*, 33–45.

Johnson, G. L., and B. C. Heezen (1967), Morphology and evolution of the Norwegian-Greenland Sea, *Deep Sea Res. Oceanogr. Abstr.*, *14*, 755–771.

Jung, W.-Y., and P. R. Vogt (1997), A gravity and magnetic anomaly study of the extinct Aegir Ridge, Norwegian Sea, *J. Geophys. Res.*, *102*, 5065–5089.

Kempton, P. D., J. G. Fitton, A. D. Saunders, G. M. Nowell, R. N. Taylor, B. S. Hardarson, and G. Pearson (2000), The Iceland plume in space and time: A Sr-Nd-Pb-Hf study of the North Atlantic rifted margin, *Earth Planet. Sci. Lett.*, *177*, 255–271.

Kempton, P. D., J. A. Pearce, T. L. Barry, J. G. Fitton, C. Langmuir, and D. M. Christie (2002), Sr-Nd-Pb-Hf Isotope Results from ODP Leg 187: Evidence for Mantle Dynamics of the Australian-Antarctic Discordance and Origin of the Indian MORB Source, *Geochem. Geophys. Geosyst.*, *3*(12), 1074, doi:10.1029/2002GC000320.

Klein, E. M., C. H. Langmuir, A. Zindler, H. Staudigel, and B. Hamelin (1988), Isotope evidence of a mantle convection boundary at the Australian-Antarctic Discordance, *Nature*, *333*, 623–629.

Kodaira, S., R. Mjelde, K. Gunnarsson, H. Shiobara, and H. Shimamura (1998), Structure of the Jan Mayen microcontinent and implications for its evolution, *Geophys. J. Int.*, *132*, 383–400.

Larsen, H. C., and A. D. Saunders (1998), Tectonism and volcanism at the Southeast Greenland rifted margin: A record of plume impact and later continental rupture, *Proc. Ocean. Drill. Program Sci. Results*, *152*, 503–533.

Malfère, J.-L. (2004), Panache mantellique et recyclage de matériel lithosphérique: Etude des isotopes Hf, Pb, Sr et Nd et des éléments en trace des basaltes néovolcaniques islandais, Ph.D. thesis, Dép. de Minéral., Univ. de Genève, Genève.

Mertz, D. F., and K. M. Haase (1997), The radiogenic isotope composition of the high-latitude North Atlantic mantle, *Geology*, *25*, 411–414.

Mertz, D. F., C. W. Devey, W. Todt, P. Stoffers, and A. W. Hofmann (1991), Sr-Nd-Pb isotope evidence against plume-asthenosphere mixing north of Iceland, *Earth Planet. Sci. Lett.*, *107*, 243–255.

Myhre, A. M., O. Eldholm, and E. Sundvor (1984), The Jan Mayen Ridge: Present status, *Polar Res.*, *2*, 47–59.

Neumann, E.-G., and J.-G. Schilling (1984), Petrology of basalts from the Mohns-Knipovich Ridge, the Norwegian-Greenland Sea, *Contrib. Mineral. Petrol.*, *85*, 209–223.

Nunns, A. (1983), The structure and evolution of the Jan Mayen Ridge and surrounding regions, in *Studies in Continental Margin Geology*, edited by J. S. Watkins and C. L. Drake, *AAPG Mem.*, *34*, 193–208.

Patchett, P. J., and M. Tatsumoto (1980), Hafnium isotope variations in oceanic basalts, *Geophys. Res. Lett.*, *7*, 1077–1080.

Patchett, P. J., W. M. White, H. Feldmann, S. Kielinczuk, and A. W. Hofmann (1984), Hafnium/rare earth element fractionation in the sedimentary system and crustal recycling into the Earth's mantle, *Earth Planet. Sci. Lett.*, *69*, 365–378.

Salters, V. J. M. (1996), The generation of mid-ocean ridge basalts from the Hf and Nd isotope perspective, *Earth Planet. Sci. Lett.*, *141*, 109–123.

Salters, V. J. M., and S. R. Hart (1989), The hafnium paradox and the role of garnet in the source of mid-ocean-ridge basalts, *Nature*, *342*, 420–422.

Salters, V. J. M., and W. M. White (1998), Hf isotope constraints on mantle evolution, *Chem. Geol.*, *145*, 447–460.

Salters, V. J. M., and A. Zindler (1995), Extreme $^{176}Hf/^{177}Hf$ in the sub-oceanic mantle, *Earth Planet. Sci. Lett.*, *129*, 13–30.

Schilling, J.-G., M. Zajac, R. Evans, T. Johnston, W. White, J. D. Devine, and R. Kingsley (1983), Petrologic and geochemical variations along the Mid-Atlantic Ridge from 29°N to 73°N, *Am. J. Sci.*, *283*, 510–586.

Schilling, J.-G., R. Kingsley, D. Fontignie, R. Poreda, and S. Xue (1999), Dispersion of the Jan Mayen and Iceland mantle plumes in the Arctic: A He-Pb-Nd-Sr isotope tracer study of basalts from the Kolbeinsey, Mohns, and Knipovich Ridges, *J. Geophys. Res.*, *104*, 10,543–10,569.

Schmidberger, S. S., A. Simonetti, D. Francis, and C. Gariépy (2002), Probing Archean lithosphere using the Lu-Hf isotope systematics of peridotite xenoliths from Somerset Island kimberlites, *Canada, Earth Planet. Sci. Lett.*, *197*, 245–259.

Simon, N. S. C., G. I. Irvine, G. R. Davies, D. G. Pearson, and R. W. Carlson (2003), The origin of garnet and clinopyroxene in "depleted" Kaapvaal peridotites, *Lithos*, *71*, 289–322.

Skogseid, J., and O. Eldholm (1987), Early Cenozoic crust at the Norwegian continental margin and the conjugate Jan Mayen Ridge, *J. Geophys. Res.*, *92*, 11,471–11,491.

Stracke, A. (2001), Mantle melting beneath Iceland and Hawaii, Ph.D. thesis, Dep. of Geol. Sci. Fla. State Univ., Tallahassee.

Stracke, A., A. Zindler, V. J. M. Salters, D. McKenzie, J. Blichert-Toft, F. Albarède, and K. Grönvold (2003), Theistareykir revisited, *Geochem. Geophys. Geosyst.*, *4*(2), 8507, doi:10.1029/2001GC000201.

Tackley, P. J., and S. Xie (2002), The thermochemical structure and evolution of Earth's mantle: Constraints and numerical models, *Philos. Trans. R. Soc. London, Ser. A*, *360*, 2593–2609.

Thirlwall, M. F. (1995), Generation of the Pb isotope characteristics of the Iceland plume, *J. Geol. Soc. London*, *152*, 991–996.

Thirlwall, M. F. (2002), Multicollector ICP-MS analysis of Pb isotopes using a ^{207}Pb-^{204}Pb double spike demonstrates up to 400 ppm/amu systematic errors in Tl-normalization, *Chem. Geol.*, *184*, 255–279.

Thirlwall, M. F., M. A. M. Gee, R. N. Taylor, and B. J. Murton (2004), Mantle components in Iceland and adjacent ridges investigated using double-spike Pb isotope ratios, *Geochim. Cosmochim. Acta*, *68*, 361–386.

Todt, W., R. A. Cliff, A. Hanser, and A. W. Hofmann (1996), Evaluation of a ^{202}Pb-^{205}Pb double spike for high-precision lead isotope analysis, in *Earth Processes: Reading the Isotope Code*, *Geophys. Monogr. Ser.*, vol. 95, edited by S. R. Hart and A. Basu, pp. 429–437, AGU, Washington, D. C.

Trønnes, R. G., S. Planke, B. Sundvoll, and P. Imsland (1999), Recent volcanic rocks from Jan Mayen: Low-degree melt fractions of enriched northeast Atlantic mantle, *J. Geophys. Res.*, *104*, 7153–7168.

van Keken, P. E., and C. J. Ballentine (1998), Whole-mantle versus layered mantle convection and the role of a high-viscosity lower mantle in terrestrial volatile evolution, *Earth Planet. Sci. Lett.*, *156*, 19–32.

van Orman, J. A., T. L. Grove, and N. Shimizu (1998), Uranium and thorium diffusion in diopside, *Earth Planet. Sci. Lett.*, *160*, 505–519.

van Orman, J. A., T. L. Grove, and N. Shimizu (2001), Rare earth element diffusion in diopside: Influence of temperature, pressure, and ionic radius, and an elastic model for diffusion in silicates, *Contrib. Mineral. Petrol.*, *141*, 687–703.

Vlastélic, I., D. Aslanian, L. Dosso, H. Bougault, J. L. Olivet, and L. Géli (1999), Large-scale chemical and thermal division of the Pacific mantle, *Nature*, *399*, 345–350.

Waggoner, D. G. (1990), An isotopic and trace element study of mantle heterogeneity beneath the Norwegian-Greenland Sea, Ph.D. thesis, Grad. School of Oceanogr., Univ. of R. I., Kingston.

White, W. M., and R. A. Duncan (1996), Geochemistry and geochronology of the Society Islands: New evidence for deep mantle recycling, in *Earth Processes: Reading the Isotopic Code*, *Geophys. Monogr. Ser.*, vol. 95, edited by A. Basu and S. R. Hart, pp. 183–206, AGU, Washington, D. C.

White, W. M., F. Albarède, and P. Télouk (2000), High-precision analysis of Pb isotopic ratios using multi-collector ICP-MS, *Chem. Geol.*, *167*, 257–270.

Zindler, A., and S. R. Hart (1986), Chemical geodynamics, *Annu. Rev. Earth Planet. Sci.*, *14*, 493–571.